A KINEMATICS-BASED MODEL OF HAND FUNCTION FOR CLINICAL EVALUATION AND DESIGN OF HANDHELD OBJECTS

By

Samuel Thomas Leitkam

A DISSERTATION

Submitted to
Michigan State University
In partial fulfillment of the requirements
for the degree of

Mechanical Engineering – Doctor of Philosophy

2014

ABSTRACT

A KINEMATICS-BASED MODEL OF HAND FUNCTION FOR CLINICAL EVALUATION AND DESIGN OF HANDHELD OBJECTS

By

Samuel Thomas Leitkam

Hand function is quantified in different ways for clinical evaluation and object design. It is measured in the clinical environment to evaluate changes in function and levels of function with respect to the population. In design, it is used to understand what healthy hands can do so that objects can be made to fit the abilities of users. However, no hand function quantification method is currently applied to both evaluation and design, allowing for design of objects for individuals with reduced functional abilities in their hands.

The goals of the research were to: 1) develop a kinematics-based model of the 3D reachable space of the fingers of the hand, weighted by objective measures of functional ability; 2) assess the model's ability to evaluate levels of function between individuals with varying levels of hand function; and 3) demonstrate that the model could be applied to a design scenario to assist in designing handheld objects for groups of individuals, specifically groups with reduced functional abilities. These goals were addressed by three different research studies.

The first study presented the mathematical development of the weighted fingertip space (WFS) model and an initial evaluation of the model as applied to a theoretical 50th percentile male hand and nine healthy individuals. The WFS model transformed hand dimensions and finger joint ranges of motion into a three-dimensional representation of all of the points in space reachable by the fingertips. The reachable points were then weighted based on the number of ways each point could be reached, the range of fingertip pad orientations possible at each point, and the range of force application directions that could be applied at each point. The results showed that the model was capable of calculating and presenting the weighted functional space, and the theoretical 50th

percentile male model showed similarities in size, shape, and weighting patterns to the models developed from the individuals with similar sized hands. In addition, the models all showed distinct spatial patterns for each of the three weighting parameters. From this, it was shown that the WFS model could have potential application in both evaluation of function and design.

The second study examined the differences between WFS models of healthy and arthritic individuals to assess the model's ability to evaluate function for clinical purposes. Hand dimensions and ranges of motion were measured for 22 healthy and 21 arthritic individuals, and WFS models were calculated for each participant. In addition, the models from the individuals were combined to evaluate whether a universally reachable space existed for each group. The results showed that the model was capable of differentiating levels of function as the arthritic group showed lower functional values than the healthy group. Further, the group models showed that a universally reachable space existed for the healthy group, but not for the entire arthritic group. However, the arthritic group's most reachable spaces overlapped with the universally reachable space of the healthy group.

The third study showed the WFS model's ability to aid in design by demonstrating that the model's 3D representation of functional weighting values could be mapped to the surface a 3D modeled handheld object and interpreted for a given task. The models developed in the second study were all mapped to the surfaces of cylinders of varying size representative of a handheld device, an auto-injector. The mappings of the model to the cylinders were used to evaluate the diameter of cylinder that best matched the abilities of the individuals. It was shown that for both the healthy and arthritic groups, the WFS models mapped the highest levels of functional weightings to the 40 mm cylinder diameter. From this research, it was shown that the WFS model can be used to evaluate handheld object designs for groups of individuals based on objective hand function quantifications.

To my family, in every form it takes

ACKNOWLEDGEMENTS

The creation and development of the work presented in this dissertation would not have been possible without the support, guidance, and love shown to me by a great many people. I would like to thank my research advisor, Dr. Tamara Reid Bush, for everything she has put forth to help this research and my career as a biomechanist come to fruition. She has been my teacher, mentor, friend, boss, therapist, and example through the entire process, and I cannot thank her enough. I would also like to thank my committee members, Dr. Laura Bix, Dr. Alejandro Diaz, and Dr. Neil Wright, for lending me their wisdom and expertise in guiding this research to its current state. I would be remiss if I did not thank all of the individuals in the Biomechanical Design Research Laboratory who have helped out along the way. Thank you to Abinand Manorama, Josh Drost, Jessica Buschman, Pan Wu, Ben Yancho, Eric Waldron, Anand Saripalli, Jeff Hall, Mike Aurino, Andrew Cooper, and Brad Rutledge. Lastly, a special thanks a go to my wife and family for their love, support, and patience. Without you, none of this would have been possible.

TABLE OF CONTENTS

LIST OF TABLES

LIST OF FIGURES

KEY TO ABBREVIATIONS

3D	Three dimensional
a	Link length in the DH convention
Ab/Ad	Abduction/Adduction
CMC	Carpometacarpal
d	Link offset in the DH convention
DIP	Distal Interphalangeal
$dMCP$	Distance from the center of the wrist to the center of the MCP joint
DP	Distal Phalanx
DP	Length of the distal phalanx
DH	Denavit-Hartenberg
DT	Thickness of the distal phalanx
FAD	Force Application Direction
F/E	Flexion/Extension
IP	Interphalangeal
MC	Metacarpal
MCP	Metacarpophalangeal
$\angle MCP$	Angle to the MCP joint from the center of the wrist with respect to the long axis of the hand
MP	Middle Phalanx
MP	Length of the middle phalanx
$\vec{\boldsymbol{O}}$	Orientation vector of the fingertip pad
$\vec{\boldsymbol{P}}$	Position vector of the fingertip pad
PIP	Proximal Interphalangeal

PP	Proximal Phalanx
PP	Length of the proximal phalanx
ROM	Range of Motion
T_{fi}	Transformation matrix of finger f about the joint i
WFS	Weighted Fingertip Space
α	Link twist in the DH convention
γ	Azimuth angle
θ	Joint angle in the DH convention
θ_{Ab}	Abduction angle at the MCP joint
θ_{AbMAX}	Maximum abduction angle at the MCP joint
θ_{DIP}	Flexion angle at the DIP joint
θ_{FL}	Flexion angle at the MCP joint
θ_{FLMAX}	Maximum flexion angle at the MCP joint
θ_{PIP}	Flexion angle at the PIP joint
ζ	Inclination angle

1. INTRODUCTION

Hand function is currently quantified for two main functions, clinical evaluation and modeling, but both have limitations that impede the combination of their understandings. Hand evaluation for monitoring of degeneration and restoration of functional abilities uses subjective self-reporting questionnaires and task-specific physical measures not easily translated to design. Modeling of hand abilities provides objective data for device design, grasp prediction, and robotic imitation, but does not include data from individuals with reduced functionality (RF). Further, while models that calculate the three-dimensional (3D) spaces that are reachable by the fingers exist, no models have weighted the reachable spaces corresponding to functional abilities of the hand.

Therefore, this research sought to develop a model of the 3D reachable space for the hand, weighted by objective measures of functionality, and show that the model can be used for both evaluation and design purposes. To accomplish this, the first goal was to develop a kinematics-based model of the space reachable by the fingertips with weightings representing abilities of the hand related to holding and grasping objects. The second goal was to assess the model's ability to evaluate functionality in the hand by applying it to experimental data from healthy and arthritic individuals and comparing the results. The final goal was to demonstrate the model's potential for design by mapping the functional abilities of individuals' hands to various digital models of a handheld device and interpreting the results in the context of the device's intended use.

The following chapters of this dissertation present the goals, methods and findings of the research in the form of three academic journal articles with the references combined to a single section at the end of the dissertation.

Chapter 2 presents the development of the weighted fingertip space (WFS) model as well as the model's initial evaluation with a sample of healthy individuals. In this section, the equations necessary for the calculation of the WFS model were developed and presented in detail. WFS models were then calculated for a theoretical 50th percentile male and nine healthy individuals, and the results were compared for similarities and differences. This research has been published in the American Society of Mechanical Engineers (ASME) Journal of Biomechanics.

Chapter 3 discusses research comparing the WFS model data from healthy individuals to model data from RF individuals. WFS models were calculated for 22 healthy and 21 RF individuals. In addition, the data from the individual models were combined for each of the groups to indicate the amount of overlapping space that was universally reachable by each group. The results from this research were interpreted in the scope of clinical evaluations.

Chapter 4 describes an example of how the WFS model can be used to evaluate varying designs of handheld devices. The WFS models for both the healthy and RF groups were mapped to the surface of a handheld device, an auto-injector modeled as a cylinder. The diameter of cylinder model was varied to identify the diameter with the highest weighting values of the WFS model mapped to the surface. The results were interpreted in the scope of designing the auto-injector to fit the abilities of individuals as well as healthy and RF groups of individuals.

The significance of this research is that it provides an understanding of the 3D kinematic functional abilities of the hand that no other method currently available for quantification of hand function can. The ability to monitor and evaluate hand function allows for objective tracking of losses and gains of hand function due to disease and injury or rehabilitation and surgery. Mapping the WFS models to 3D-modeled objects allows for the design of objects to match the abilities of the hand. Lastly, combining the quantification of reduced hand functionality with object mapping enables the design of handheld objects catered specifically to groups of individuals with reduced hand functionality.

2. DETERMINING FUNCTIONAL FINGER CAPABILITIES OF HEALTHY ADULTS: COMPARING EXPERIMENTAL DATA TO BIOMECHANICAL MODEL[1]

2.1 Introduction

The human hand is in continuous use throughout the day. As people age, are injured, or experience disease, the functional abilities of their hands can decrease significantly. The loss of hand function is problematic in many ways. For example, people with arthritis of the hand have functional limitations that impact their daily activities. In addition to joint pain, they experience lack of overall strength, weakened grip, limited pinch strength and diminished manual dexterity [1–3]. All of these factors impact their ability to live independently as they may not be able to perform activities of daily living such as opening food and medication packages, opening doors, or zipping, snapping, or buttoning up clothing because of the disease [2,4]. Further, injury and disease may require individuals to have a joint replacement in their finger or to undergo hand therapy in order to regain lost function. Generally, loss of function, as well the recovery of function through surgery or therapy is monitored through observation of tasks and questionnaires [5,6]. Furthermore, a need exists to improve designs of packages and everyday devices, particularly for those with disabilities [7–9]. To improve design and better understand changes in hand function that occur with medical interventions, it is first necessary to understand and define the functional abilities of a normative population. This can be accomplished through a combination of model development and experimental data collection.

Currently, there are no hand models that can be used to both document functional abilities and design for functional ability. Researchers have evaluated functional capacity of the hand using strength [10–12] and some limited kinematic approaches [13–15], but these measures communicate little about the potential of the hand and how it can be used. Researchers have also evaluated aspects of the hand in terms of possible reach [16–20], but these methods have not included any associated fingertip orientation or force directionality associated with the fingers. Thus, there is a need to develop a framework that can determine regions of finger utility and weight them for functional ability for the entire hand and to compare this framework to experimental data sets.

The objectives of this work were twofold: 1) to develop a theoretical model of a 50th percentile hand that defines the reachable space and is weighted to represent three types of functionality, and 2) to compare the outcomes of this model to an experimental data set obtained from a healthy hand population. The model that was developed yielded a three-dimensional (3D) space and associated weighted vector cloud, termed a Weighted Fingertip Space (WFS), and was designed to identify all possible motions and force directions of all five fingertips for each point within a 3D mesh grid. The points within this grid were weighted based on the following three parameters: 1) the relative ability of the fingers to reach each point in space, 2) the range of possible fingertip orientations at each point, and 3) the range of force application directions at each point.

This work is novel in that it moves beyond identifying basic reachable spaces to include functional factors that can be used to monitor the efficacy of rehabilitative approaches, changes in function pre and post-surgical interventions and to design handheld objects that match the capabilities of users – including those with reduced abilities. This approach also offers insight into why some finger postures and corresponding fingertip positions may be used more frequently than others.

2.2. Methods

2.2.1 Theoretical Hand Model

Rigid links

The hand was considered as a system of sixteen rigid bodies. The rigid bodies were: the palm; the first metacarpal; the proximal and distal phalanges of the first digit (thumb); and the proximal, middle and distal phalanges of the second through fifth digits (i.e. index finger through little finger), Figure 1. Each rigid body was treated as a three dimensional solid object.

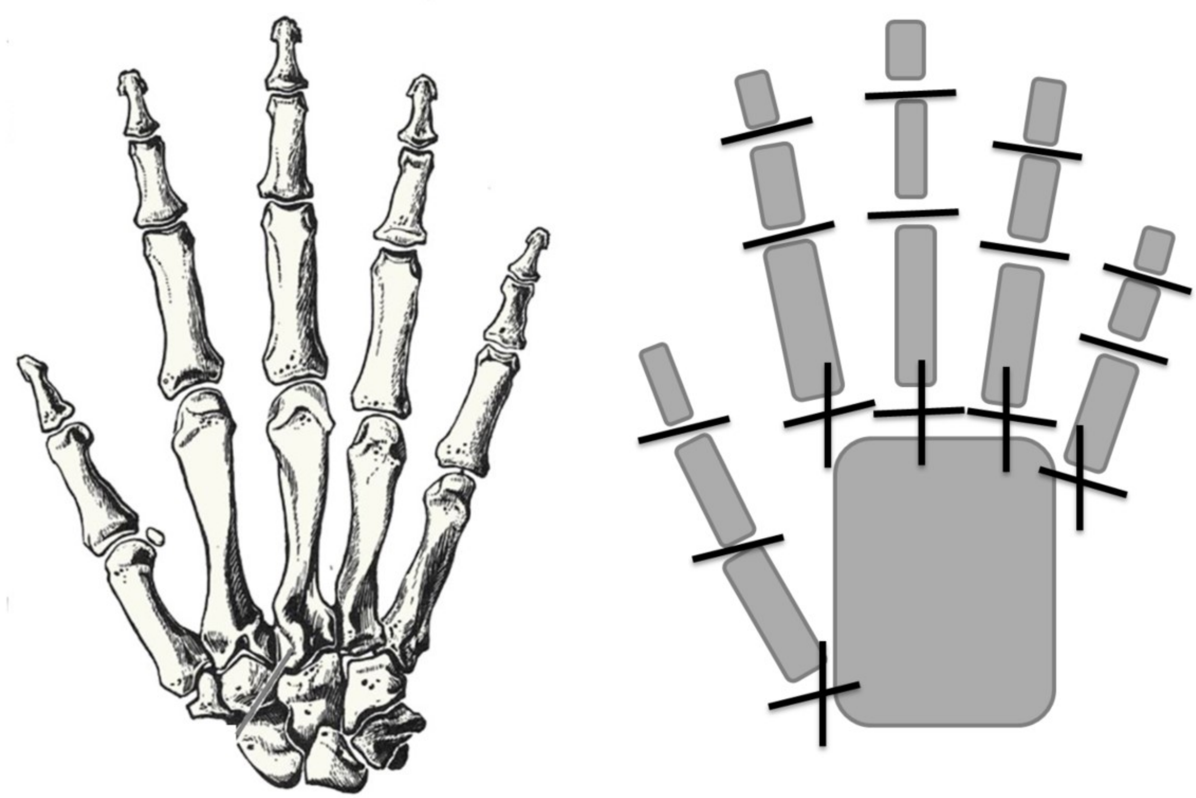

Figure 1. Diagram of the rigid bodies used in the hand model. (Left) Bones of the right hand (Right) Gray boxes represent the corresponding rigid bodies and black lines represent the axes of rotation and therefore, the degrees of freedom of the joints linking the rigid bodies together.

The dimensions for each rigid body were taken from previously published literature [21] for the initial theoretical model. Though the human hand varies in size from individual to individual, the dimensions of the hand have been studied in detail and have been statistically organized into groups based on gender and size. In order to provide a baseline, the 50th percentile male hand size was used.

Thirty dimensions quantified the rigid bodies. The dimensions included the distal and medial/lateral lengths from the center of the wrist to the "base joint" of each finger (carpometacarpal joint for thumb, metacarpophalangeal joints for index through little finger), the length of the first metacarpal, lengths of the all of the phalanges, and palmar/dorsal thickness of the distal phalanges, Figure 2.

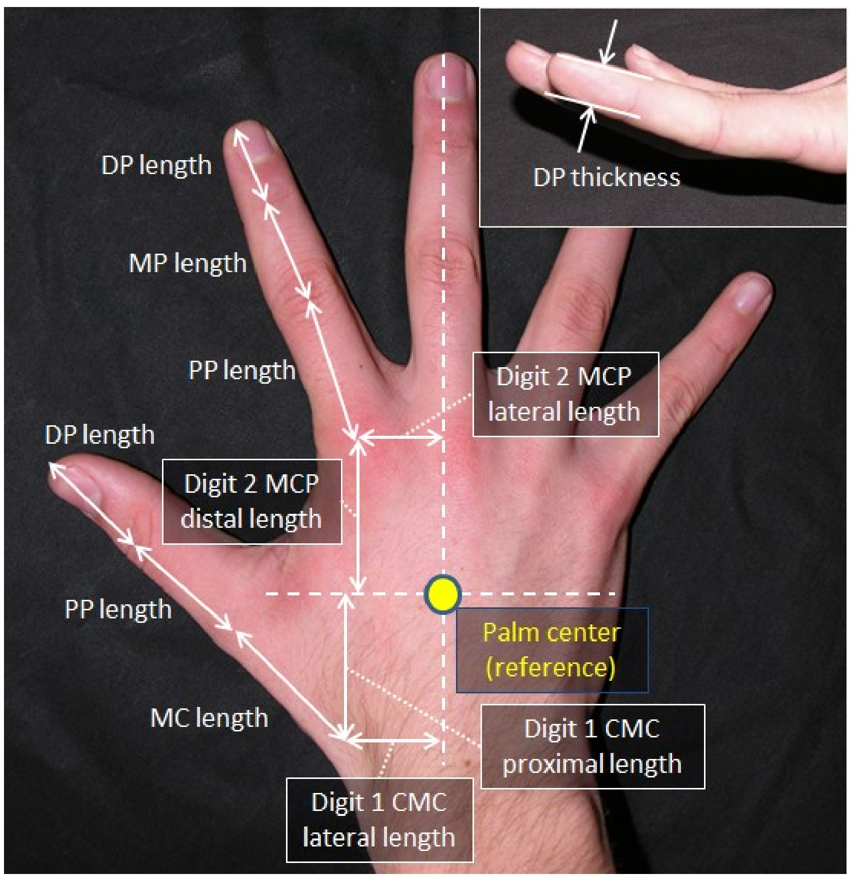

Figure 2. Hand dimensions used for the rigid bodies of the model. The dimensions for rigid bodies of digits three through five were taken similarly as those shown for digit two.

Degrees of Freedom

The rigid bodies of the hand model were linked together with 20 rotational joints. Limitations of movement were imposed so that movements of the model resembled the mobility of the fingers. For the second through fifth digits, mobility included flexion/extension (F/E) and abduction/adduction (Ab/Ad) motions about the metacarpophalangeal (MCP) joints, as well as F/E at the proximal interphalangeal (PIP) joints and distal interphalangeal (DIP) joints. For the first digit, the thumb, mobility included F/E motions at the MCP joint and the interphalangeal (IP) joint as well as two different rotations at the carpometacarpal (CMC) joint. The range of motion (ROM) data for the joints were taken from the Merck Manual for Health Care Professionals [22].

Due to redundancy in anatomical naming of the motions of the first CMC joint in anatomical nomenclature, an engineering-based terminology was used for this joint. To describe movements of the thumb at the CMC joint, a spherical coordinate system was utilized. The coordinate system was oriented with the origin at the CMC joint, the zenith axis parallel to the long axis of the hand, and the azimuth angle as measured from the plane of the hand. As such, rotations of the metacarpal away from the zenith axis (abduction and extension in anatomical terminology) were deemed changes in the inclination angle (ζ). Rotations of the metacarpal bone about zenith axis away from the plane of the palm (flexion and opposition in anatomical terminology) were deemed changes in the azimuth angle (γ), Figure 2.

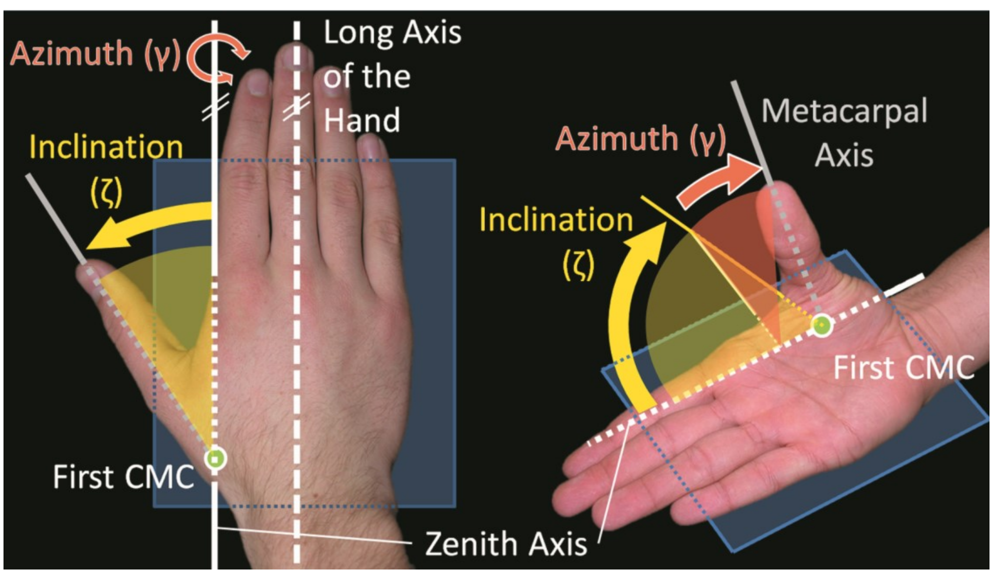

Figure 3. Thumb CMC motion terminology. The zenith axis was a line parallel to the long axis of the hand and running through the center of the CMC joint. The inclination angle (ζ) was the angular amount of rotation of the thumb away from the zenith axis. The azimuth angle (γ) was the angular amount of rotation of the thumb about the zenith axis where 0 degrees indicated the thumb being in the plane of the hand.

Motion Dependency

Two movement constraints were included in the development of the WFS model. The constraints were implemented to reduce the possibility of overestimating the functional ranges of finger movement. The first movement constraint that was included affects the movement of the DIP and PIP joints in digits two through five and states that in free movement, without any external load applied to the finger, the DIP movement may not exceed two-thirds the value of the PIP motion. This has been used previously in hand research [23,24] and is modeled by Eq. (1).

$$\theta_{DIP} \leq 2/3\ \theta_{PIP} \tag{1}$$

The second movement constraint that was included in the model addresses the relative movement of the MCP Ab/Ad and F/E motions of digits two through five and states that as the MCP joint is flexed from a straightened finger to maximum flexion, the allowable amount of Ab/Ad decreases from the maximum ROM to 0 degrees of ROM [24], shown for abduction in Eq. (2). The same principles were applied for abduction and adduction.

$$\theta_{Ab} \leq (1-1/\theta_{FLMAX})\ \theta_{AbMAX} * \theta_{FL} \tag{2}$$

2.2.2 Calculation of Fingertip Pad Positions, Orientations, and Force Application Directions

Determining Equations for Positions and Orientations of the Fingertip Pads

Coordinated movements of several joints of each finger result in complex motions of the fingertip with respect to the planes of the hand [25], and thus require a detailed technique to accurately track the fingertip position through joint angle changes. The Denavit-Hartenberg (DH) convention is a common approach used to calculate the position and orientation of the end of a multi-link system that moves through a set of rotations and translations [26,27]. This convention originated for use in robotics but has been adopted in biomechanics research [19,28–30]. Similarly, for the current research, the DH approach was used to identify the reach space of each finger, and form the kinematic aspect of the weighted fingertip space (WFS).

The DH variables represented distinct values that related the local coordinate systems of the rigid body finger segments to each other for a given digit. There were no translational joints in the hand model (all joints were rotational joints) so the link length, labeled “a”, and link offset, labeled “d ”, were assigned fixed values based on the physical dimensions of the hand and the link twist, labeled “α ”, was assigned fixed values that related the relative twist between two adjacent local coordinate systems. The joint angle, labeled “θ”, was considered the variable of motion and corresponded to an angle within the joint’s range of motion. The values that described the variables for the transformations in digit two are presented in Table 1. These values were similarly determined for digits three through five.

Table 1. Values for Denavit-Hartenberg transformation variables applied to the second digit. The left column indicates what transformation was occurring, and the associated row indicates the values used for each variable.

	Transformation #, i	a_{2i} (mm)	d_{2i} (mm)	α_{2i} (deg.)	θ_{2i} (deg.)
Palm to MCP Ab/Ad	1	$dMCP_2$	0	0	$-\angle MCP_2$
MCP Ab/Ad to MCP F/E	2	0	0	90	$\angle MCP_2+\theta_{21}$
MCP F/E to PIP F/E	3	PP_2	0	0	θ_{22}
PIP F/E to DIP F/E	4	MP_2	0	0	θ_{23}
DIP F/E to Fingertip Pad	5	$DP_2/2$	$DT_2/2$	-90	θ_{24}

The transformation from one local coordinate system to the next was described using a 4x4 matrix. The basic transformation matrix can be seen as Eq. (3) where f indicates the finger (f=1-5, thumb to little finger) and i indicates the transformation (joint rotation or translation) number within that finger (i=1-5, corresponding to Table 1).

$$T_{fi} = \begin{bmatrix} cos\theta_{fi} & -sin\theta_{fi} * cos\alpha_{fi} & sin\theta_{fi} * sin\alpha_{fi} & a_{fi}cos\theta_{fi} \\ sin\theta_{fi} & cos\theta_{fi} * cos\alpha_{fi} & -cos\theta_{fi} * sin\alpha_{fi} & a_{fi}sin\theta_{fi} \\ 0 & sin\alpha_{fi} & cos\alpha_{fi} & d_{fi} \\ 0 & 0 & 0 & 1 \end{bmatrix} \tag{3}$$

Mapping the values for the transformations in Table 1 to Eq. (3) resulted in the transformation matrices shown in Eqs. (4-8). Similar mapping of the values to Eq. (3) was performed for the thumb transformations with the only difference being the values for "a","d ", "α ", and "θ ".

$$T_{21} = \begin{bmatrix} cos(\angle MCP_2) & sin(\angle MCP_2) & 0 & dMCP_2 * cos(\angle MCP_2) \\ -sin(\angle MCP_2) & cos(\angle MCP_2) & 0 & -dMCP_2 * sin(\angle MCP_2) \\ 0 & 0 & 1 & 0 \\ 0 & 0 & 0 & 1 \end{bmatrix} \tag{4}$$

$$T_{22} = \begin{bmatrix} cos(\angle MCP_2 + \theta_{21}) & 0 & sin(\angle MCP_2 + \theta_{21}) & 0 \\ sin(\angle MCP_2 + \theta_{21}) & 0 & -cos(\angle MCP_2 + \theta_{21}) & 0 \\ 0 & 1 & 0 & 0 \\ 0 & 0 & 0 & 1 \end{bmatrix} \tag{5}$$

$$T_{23} = \begin{bmatrix} cos\theta_{22} & -sin\theta_{22} & 0 & PP_2 * cos\theta_{22} \\ sin\theta_{22} & cos\theta_{22} & 0 & PP_2 * sin\theta_{22} \\ 0 & & 1 & 0 \\ 0 & 0 & 0 & 1 \end{bmatrix} \tag{6}$$

$$T_{24} = \begin{bmatrix} cos\theta_{23} & -sin\theta_{23} & 0 & MP_2 * cos\theta_{23} \\ sin\theta_{23} & cos\theta_{23} & 0 & MP_2 * sin\theta_{23} \\ 0 & 0 & 1 & 0 \\ 0 & 0 & 0 & 1 \end{bmatrix} \tag{7}$$

$$T_{25} = \begin{bmatrix} cos\theta_{24} & 0 & -sin\theta_{24} & (DP_2 * cos\theta_{24})/2 \\ sin\theta_{24} & 0 & cos\theta_{24} & (DP_2 * sin\theta_{24})/2 \\ 0 & -1 & 0 & DT_2/2 \\ 0 & 0 & 0 & 1 \end{bmatrix} \tag{8}$$

These transformation matrices (T_{f1}-T_{f5}) were then multiplied in sequence (from proximal to distal) to calculate the combined transformation matrix. This resulted in the fingertip pad position, "$\vec{\boldsymbol{P}}$", and orientation with respect to the origin at the center of the palm, "$\vec{\boldsymbol{O}}$", as functions of the joint angles.

$$T_f = T_{f1} * T_{f2} * T_{f3} * T_{f4} * T_{f5} \tag{9}$$

$$\vec{\boldsymbol{P}}(\theta_{f1},\theta_{f2},\theta_{f3},\theta_{f4}) = T_f * \begin{bmatrix} 0 \\ 0 \\ 0 \\ 1 \end{bmatrix} = \begin{bmatrix} x(\theta_{f1},\theta_{f2},\theta_{f3},\theta_{f4}) \\ y(\theta_{f1},\theta_{f2},\theta_{f3},\theta_{f4}) \\ z(\theta_{f1},\theta_{f2},\theta_{f3},\theta_{f4}) \\ 1 \end{bmatrix} \tag{10}$$

$$\vec{\boldsymbol{O}}(\theta_{f1},\theta_{f2},\theta_{f3},\theta_{f4}) = T_f * \begin{bmatrix} 0 \\ 0 \\ 1 \\ 0 \end{bmatrix} = \begin{bmatrix} u(\theta_{f1},\theta_{f2},\theta_{f3},\theta_{f4}) \\ v(\theta_{f1},\theta_{f2},\theta_{f3},\theta_{f4}) \\ w(\theta_{f1},\theta_{f2},\theta_{f3},\theta_{f4}) \\ 0 \end{bmatrix} \tag{11}$$

Similar calculations were performed for digits one, and three through five yielding similar equations for the fingertip pads' positions and orientations.

Determining Equations for Force Application Directions

Fingertip pad force application directions (FADs) were calculated for each possible fingertip position and orientation. Each FAD corresponded to a theoretical flexion movement of one of the joints of the finger (MCP, PIP, and DIP) and represented the direction in which a grasping or button actuation force could be generated at the fingertip pad. The flexion motions were chosen for this calculation as they represented the primary motions used to close the fingers around an object or press a button.

The FADs were determined to be the gradient of fingertip pad position with respect to the flexion joints of the finger, Eq. (12).

$$FAD_{\theta fi} = \frac{\partial(\vec{\boldsymbol{P}})}{\partial(\theta_{fi})} \tag{12}$$

In physical space, the FADs corresponded to the tangential direction to a circle centered at the rotational joint centers of the finger and oriented in the F/E plane of the finger. A diagram of the three FADs for a single finger orientation of the second digit can be seen in Figure 3.

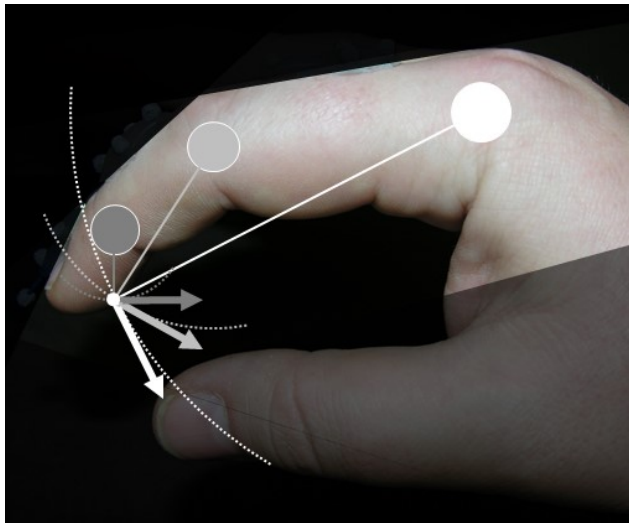

Figure 4. Diagram of the three possible FADs for a fingertip position/ orientation of the second digit. Each position, force direction and movement arc are coordinated by shades of gray.

Sampling the Joint ROMs to Determine WFS

The joint angle ROMs were sampled to yield discrete sets of joint angles that could be used in the equations for determining the possible fingertip positions, orientations and FADs. The joint angle sets were chosen to represent every possible unique integer combination of the four joint angles for each finger. To account for the motion dependency limitations, each set of angular values was then checked against Eq. (1) and Eq. (2) and any sets that did not fit the requirements were omitted. The remaining angular combinations were then each input into the equations for position, orientation, and FADs. The 3D volume containing the fingertip positions and vectors was determined to be the reachable space of the WFS. Figure 4 presents a 2D plot of these data. All calculations and plotting of the WFS were performed in MATLAB, a numerical computing software package.

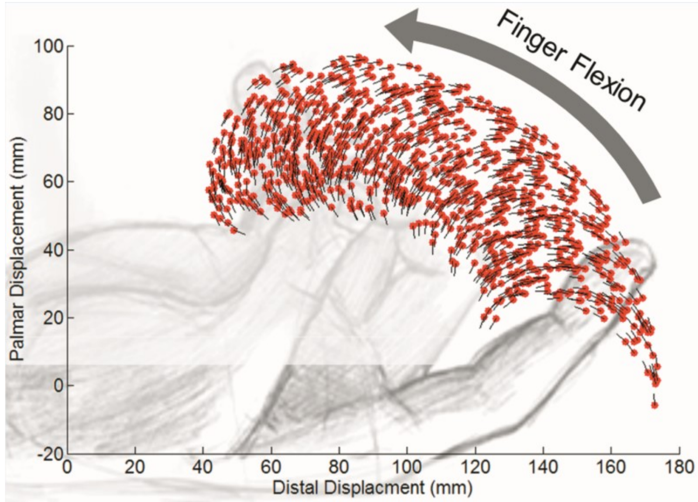

Figure 5. Visual representation of the possible fingertip pad positions and orientations of the second digit calculated in the WFS, shown as a plane bisecting the second digit. Red dots indicate the fingertip pad positions, while black lines indicate the normal direction pointing out of the face of the fingertip pad at those points. Only 1,000 points are shown for clarity, and the gray finger shown in background is included to show orientation in space with respect to the hand.

2.2.3 Weighting the WFS

To facilitate weighting of the WFS, the calculated fingertip positions were rounded to the nearest 2.5mm in the X, Y, Z global coordinate system. In space, this corresponded to translating each vector to the nearest point in a 3D mesh. A plot of the grouped WFS position and orientation data are shown in Figure 5.

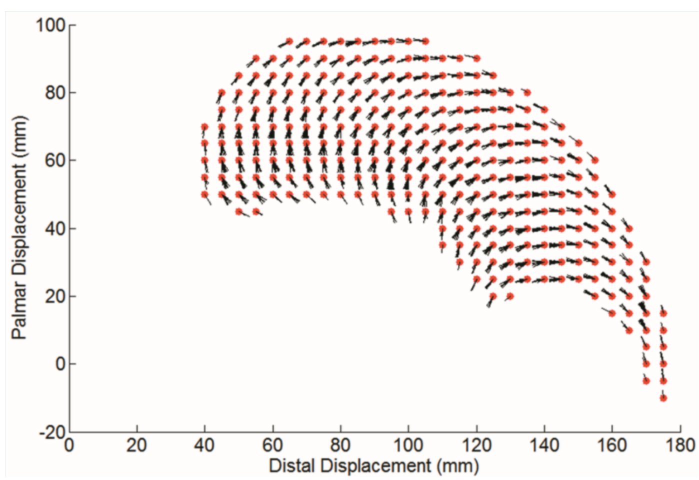

Figure 6. Clustered WFS where the position points and orientation vectors have been grouped to the nearest mesh point. Red dots indicate the rounded fingertip pad positions, while black lines indicate the normal directions pointing out of the face of the fingertip pad at those points. Finger orientation is the same as depicted in Figure 4.

For this research, the reachable space of the hand was weighted corresponding to three weighting parameters. The weighting parameters were: 1) the relative number of possible ways a finger could reach a particular point in the WFS; 2) the range of fingertip orientations that were possible at a particular point in the WFS; and 3) the range of directions of possible force application at a particular point in the WFS. These three weighting parameters were selected because each could be related to an aspect of hand functionality.

Number of Ways to Reach Weighting

The *Number of Ways to Reach* weighting was identified by the number of vectors collected at each mesh point and lent insight into the number of possible ways that a single finger could reach a particular point in the WFS. The rationale for including this parameter was to obtain data on how many unique combinations of joint angles, or finger postures, would result in a fingertip reaching a given point. This has direct relevance for design, in that WFS mesh points that exhibited lower values were reachable by fewer unique finger postures. Higher values were given to mesh points in the WFS with a higher number of finger postures resulting in the fingertip pad being positioned at that mesh point. For example, a value of "one" would indicate that there was only one angular combination or finger posture that resulted in the fingertip ending in that particular 2.5mm x 2.5mm x 2.5mm volume.

Fingertip Orientation Range Weighting

The *Fingertip Orientation Range* weighting parameter was based on the range of fingertip orientation vectors collected at each mesh point. At each reachable mesh point in the WFS the two orientation vectors that formed the limits of the angular range were identified and the angle between the limiting vectors was calculated. This range value was then used as the weighting of that particular mesh point. The rationale for including this parameter was to provide a data set that can help determine the points in space where the fingertip pad is highly adaptable to match a range of surface contours. Higher values represented points where the fingertip could be oriented in a wide range of orientations, whereas smaller values represented points where the fingertip could only be oriented in a single direction or very similar directions.

Force Application Direction (FAD) Range Weighting

The *FAD Range* weighting parameter of the WFS was based on the ranges of possible FADs available at each mesh point. This weighting parameter was determined by identifying the two FAD vectors that were the limits of the range and calculating the angle between them. The rationale for this parameter was to identify the range of directions where forces could be applied to an object in a given finger posture. Higher values represented points where the fingertip could apply force in a wide range of directions, whereas smaller values represented points where the fingertip could only apply force in a single direction or very similar directions. For example, an index finger at full extension can only apply forces in a very small range of vector directions, meaning that if any force direction other than that is needed, the other joints (wrist, elbow, shoulder, etc.) must supply the additional motion. In contrast, the fingertip of a partially flexed finger has a wider range of force application directions, so the direction of force can changed using just joints of the finger.

2.2.4 Experimental Data Collection for Individualized WFS Models

In addition to the theoretical model developed from the 50th percentile hand size, nine healthy participants were measured for the experimental data collection and development of individualized WFS models. Five women and four men with average age of 27.2 (SD 3.3) and no reported injury to the elbow, wrist, or hand were tested (IRB 09-179). The women had an average height of 1.63 m (SD 0.68 m), average mass of 67.6 kg (14.3 kg), and average hand breadth of 77.0 mm (SD 4.4 mm). The men had an average height of 1.76m (SD 0.14 m), average mass of 94.1 kg (32.9 kg), and average hand breadth of 87.8 mm (SD 7.2 mm). Anthropometric data and angular ranges of motion of the individuals' right hands were measured and then used to calculate a WFS model for each participant, with corresponding weightings. Though the dominant hand was noted, all measurements were made of the right hand. Testing of only the right hand was conducted to streamline the data collection, keep the testing time to 2 hours or less, and for ease of data processing. All but one of the participants was right-handed.

Hand Measurements

Anthropometric measurements were taken for each participant. These measurements included all of the dimensions necessary for the WFS model calculation, and were obtained with an electronic caliper system accurate to 0.01mm (Starrett Model 723). The dimensions measured were: hand breadth, hand length, length of each phalanx, and thickness of each fingertip. Additionally, the distal and lateral lengths from a point on the center of the palm to the origin of each finger's base joint (CMC joint for the first digit and to the MCP joints for digits two through five) were measured. These measures established each finger's position with respect to one another for use in determining the link attachment positions to the palm in the model. A diagram of these measurements is located in Figure 1.

Joint Angle Calculations

To determine each individual's WFS, joint ranges of motion for each participant's fingers were calculated. Ranges of motion for each finger were measured using a seven-camera motion capture system (Qualisys, Gothenburg, Sweden) in conjunction with 64 retro-reflective markers. Analogous to the hand model for calculation of the WFS, each individual's hand was considered a system of 16 rigid bodies (three links for each finger and one for the palm). Each rigid body was tracked as a six degree of freedom body using a rigid pod of four markers while the fingers moved through their full ranges of motion. Fourteen pods of 4mm diameter markers were affixed to the phalanx segments of the fingers to measure the relative motions of the phalanges, Figure 6. Two pods of 6mm diameter markers were affixed to the posterior side of the hand, one centered over the third metacarpal and one centered over the first metacarpal to measure the position of the base of the hand and the motion of the first metacarpal.

Figure 7. Hand with marker pods used for calculation of finger joint ROMs.

To calculate the full ROM for the joints, each participant was asked to perform seven prescribed hand motions designed to illicit the maximum range of motion at each of the joints. The motions were:

1. MCP Flexion- Participants were asked to "fold" their right hand closed so their fingertip pads rested flat on the base of the palm, as near the wrist as possible, and to focus on creating as much flexion in the MCP joints as possible. An example of the end position of this motion is shown in Figure 8. This motion was used to measure the maximum flexion in the MCP joints of digits two through five.

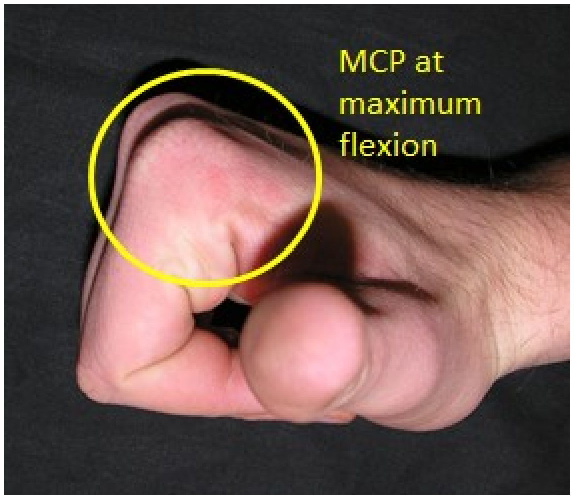

Figure 8. Final hand position for MCP flexion motion.

2. Maximum PIP and DIP Flexion- Participants were asked to "curl" their fingers as much as possible so their fingertip pads rested flat on the anterior surface of their proximal phalanges and to focus on creating as much flexion in the DIP joints as possible, while minimizing MCP flexion. An example of the end position of this motion is shown in Figure 9. This motion was used to measure the maximum flexion in the PIP and DIP joints of digits two through five.

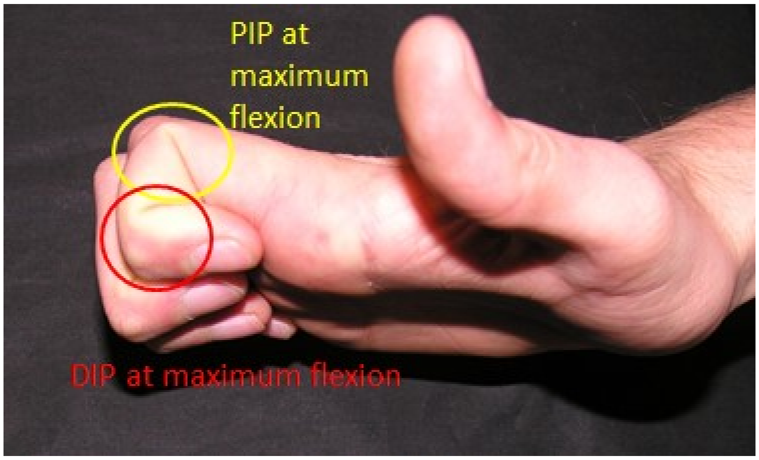

Figure 9. Final hand position for PIP and DIP flexion motion.

3. Maximum Finger and Thumb Extension- Participants were asked to extend their fingers as much as possible, as seen in Figure 10. This motion was used to measure the maximum extension (minimum flexion) at the MCP, PIP, and DIP joints of digits two through five and MCP and IP joints of the thumb.

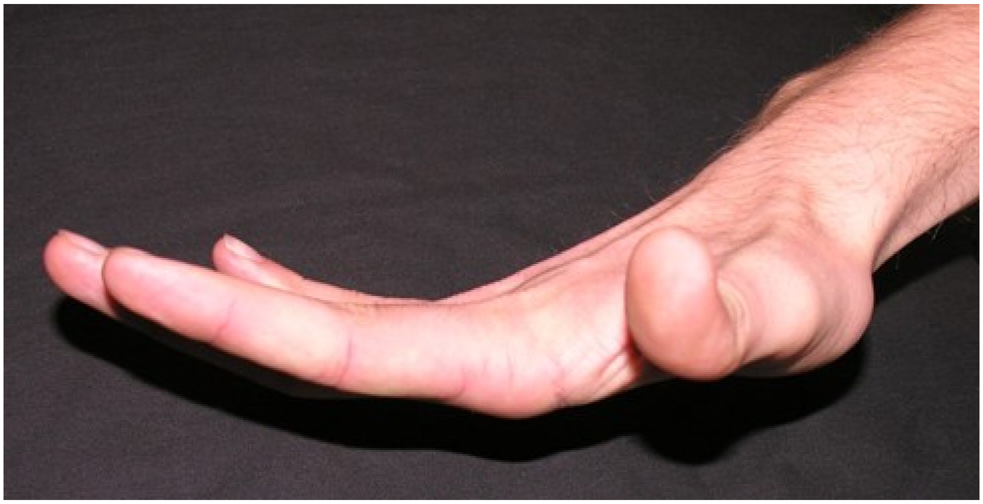

Figure 10. Final hand position for finger and thumb extension motion. Maximum extension is shown for all finger joints (MCP, PIP, DIP) and thumb joints (MCP, IP).

4. Maximum Finger Abduction/Adduction - Participants were asked to “spread” their fingers in four ways: separating second and fifth digit as much as possible, separating second and third as much as possible, separating third and fourth as much as possible and separating

fourth and fifth as much as possible. The four configurations are shown in Figure 11. These motions were used to measure the maximum abduction and adduction in each finger at the MCP joint of digits two through five.

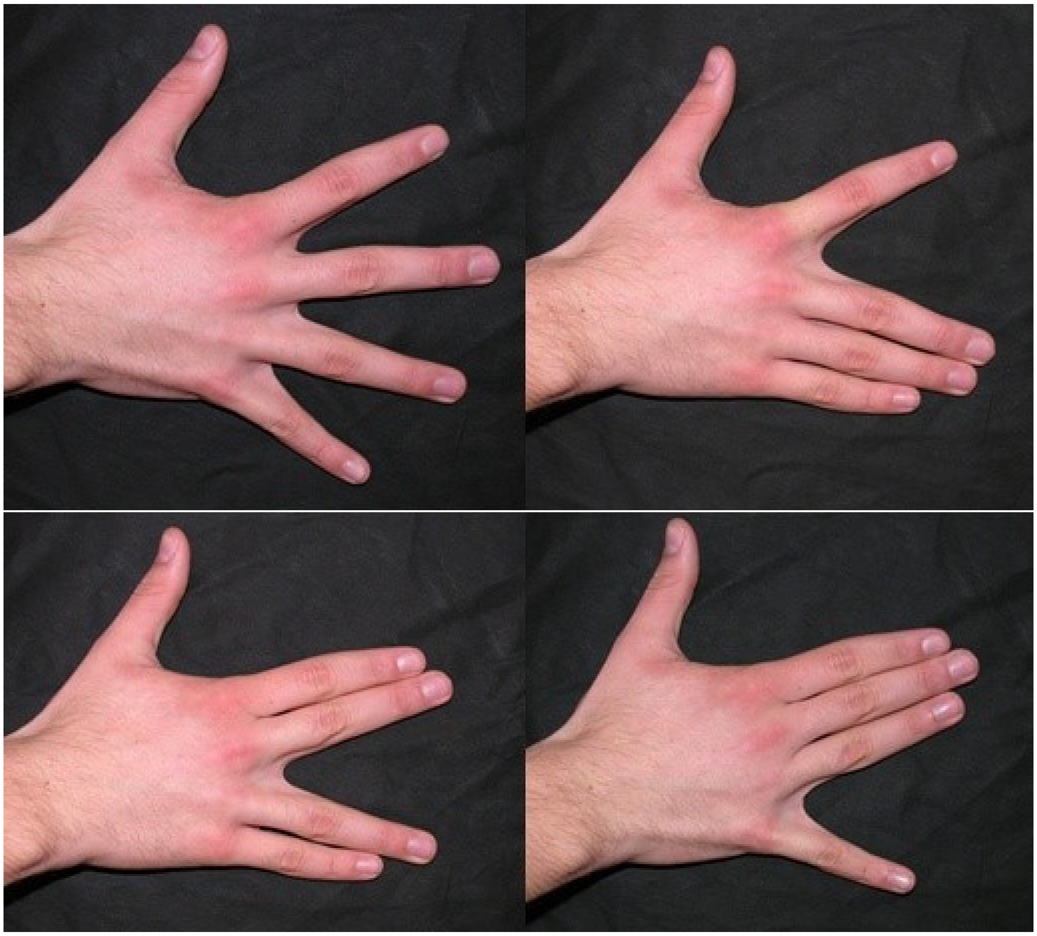

Figure 11. Final hand positions for finger abduction/adduction motions. Clockwise from top left: separating second and fifth digits, separating second and third digits, separating third and fourth digits, separating fourth and fifth digits.

5. Thumb Flexion- Participants were asked to flex their thumbs as much as possible at the MCP and IP joints, as seen in Figure 12. This motion was used to measure the maximum flexion at the MCP and IP joints of the thumb.

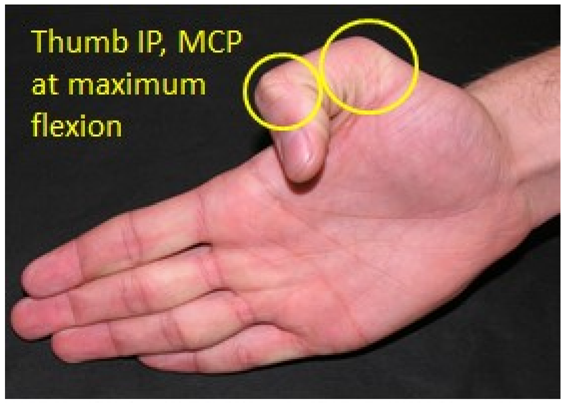

Figure 12. Final hand position for thumb flexion motion

6. Thumb Azimuth Rotation (CMC rotation around hand) - Participants were asked to make as large of an arc as possible while moving the tip of their thumbs from a position in plane with the palm, spread away from the index finger, to touching their palms on the ulnar side of the hand, Figure 13. This motion was used to measure the maximum and minimum azimuth angles and maximum inclination angles possible at the CMC joint of the thumb.

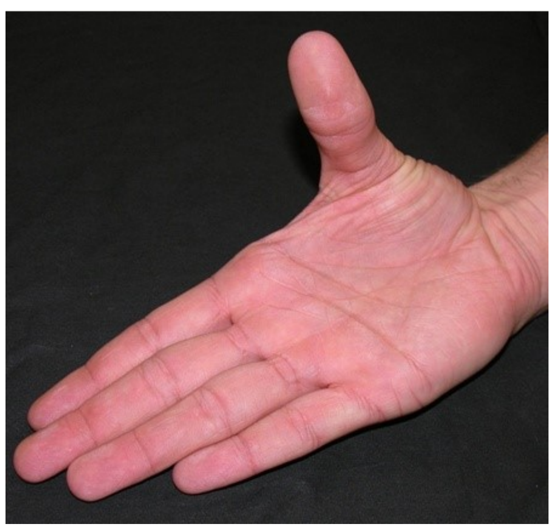

Figure 13. Mid-motion hand position for thumb azimuth rotation motion

7. Thumb Palm Arc (CMC rotation across palm) - Participants were asked to bring their thumbs toward their palms and rotate about the CMC such that the thumb moved across the distal palmar surface of the hand moving from the index to little finger. An example of the end position can be seen in Figure 14. This motion was used to measure the minimum inclination angle at the CMC joint of the thumb.

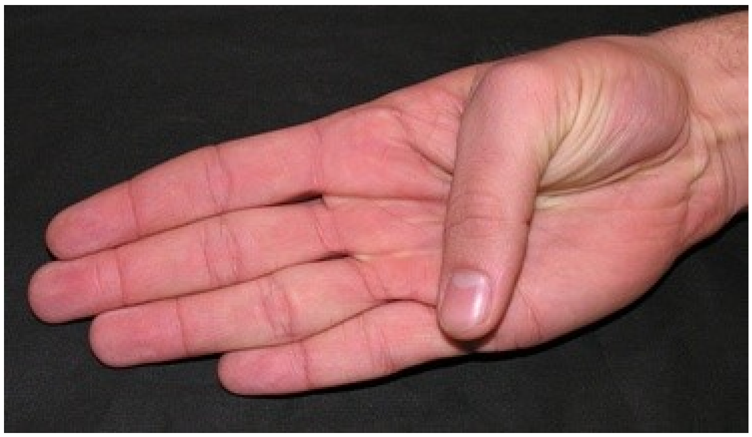

Figure 14. Final hand position for thumb palm arc motion

For the data collection, the participants were seated in an office chair with armrests, and the right hand was positioned in unobstructed space with the elbow at a 90 degree angle. The palm of the hand was oriented in a vertical plane with the thumb pointing in an upward direction. Each intended motion was clarified with each participant through verbal communication, physical demonstration, and practice before collection of the data. For each trial, the finger motion was performed twice in a continuous motion starting from an initial reference position, moving to the posture that produced the maximum joint angle, and then back to the original posture. Two trials of each motion were recorded at 60Hz. Only right hand motions were measured to standardize the data collection and processing. In addition, a static file was collected with the hand flat (palm down) on a surface with the fingers aligned parallel to the long axis of the hand, and the thumb at an angle 45 degrees with respect to the long axis of the hand. This hand posture was used as the "neutral" position of the hand for the angular measurements, Figure 15.

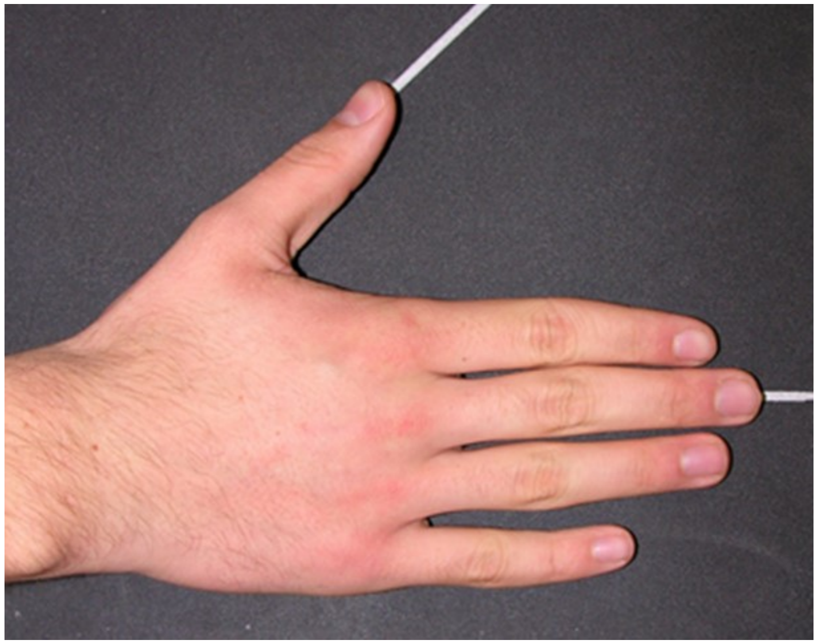

Figure 15. "Neutral" hand position with palm and fingers flat on surface, fingers pointing in a distal direction and thumb 45 degrees from the orientation of the fingers.

In order to make the required angular calculations at each joint, a local coordinate system was established on each rigid body using the marker pods. These local coordinate systems were chosen in accordance with the standards set forth by the International Society of Biomechanics (ISB) for coordinate systems of the upper limb [31]. The marker pods on the phalanges were positioned such that two of the markers were oriented along the long axis (proximal/distal) of the bone. The vector from the distal marker to the proximal marker was used as the Y-axis of the local coordinate system. The third marker on each of the pods was positioned such that, when combined with the first two markers, the three markers created a frontal plane of the hand (a plane that could separate anterior and posterior portions of each phalange). This third marker was used to identify the orientation of the Z-axis as pointing orthogonally from the Y-axis toward the radial (thumb) side of the hand. The X-axis was then determined to be the cross product of the Y and Z unit axes, pointing in the palmar direction. The local coordinate systems for the second digit are shown in Figure 7. The fourth marker was used primarily to assist the motion capture system in auto-identifying each local coordinate system uniquely, but was also used to maintain data collection if one of the other markers became occluded. The local coordinate systems for the palm, and first metacarpal were established in a similar manner, in accordance with the ISB standards [31].

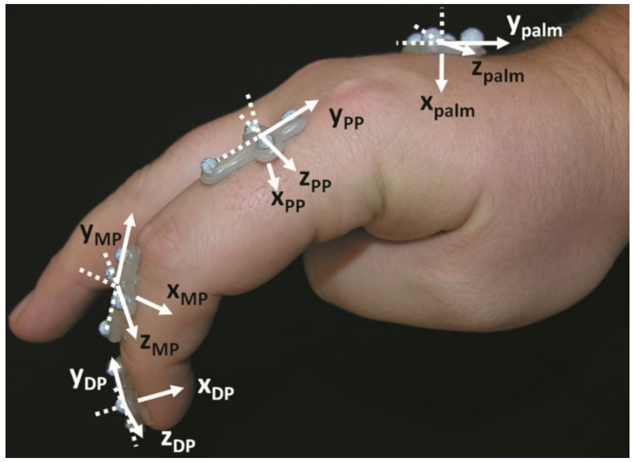

Figure 16. Local coordinate systems shown for second digit. Subscripts refer to the rigid body that the coordinate system is attached to: PP=Proximal Phalange, MP=Middle Phalange, DP=Distal Phalange

Once the local coordinate systems were established for each finger segment, the angular calculations for each joint were made using Euler angle transformations. Euler angles were chosen for this research as the angular transformations are made with respect to the local coordinate system axes. The order of rotation transformations for the finger joints were chosen to be Z, X, Y, such that F/E was calculated first, followed by Ab/Ad, and axial rotation third. For the MCP joint of the thumb, the inclination angle was calculated first, followed by the azimuth angle and the axial rotation. The orders were chosen so that the primary motions of the hand were calculated first, minimizing errors inherent with Euler angle calculations.

2.2.5 Individual WFS Model Characteristics

So that the functional abilities of the test population could be described, individual WFSs were characterized using comparison measures based on the WFS weighting parameters. There were four model measures calculated for each finger in each individual WFS: 1) the total volume of reachable space that was encapsulated by the WFS, 2) the most accessible point within the WFS, 3) the maximum range of orientation vectors at the reachable points within the WFS, and 4) the maximum range of FADs at the points within the WFS.

Total Volume of the WFS

The volume of each WFS model was calculated to provide a single value quantifying the amount of space that a person could reach with his/her fingertips. It was calculated by multiplying the number of reachable mesh points by the size of the volume accounted for by each mesh point. A larger volume indicated higher overall potential functional capacity to reach points in space.

Most Accessible Point in the WFS

The most accessible point was determined to be the mesh point that was reachable by the highest number of angular combinations. A larger value indicated a higher level of redundancy in ways for the finger to orient to reach a particular point.

Maximum Range of Orientation Vectors

The maximum range of orientation vectors of each WFS model was calculated to be a single value that represented the maximum orientation range of the all the points that could be reached by the fingertip. It was calculated by finding the point in the WFS that showed the maximum range of orientation angles. A larger maximum orientation angle indicated a higher peak level of potential functional capacity of the finger to orient the fingertip within the WFS.

Maximum Range of FADs

The maximum range of FADs of each WFS model was calculated to be a single value representing the maximum range of FADs found within the WFS model. It was calculated by finding the point that showed the largest angle between FAD vectors in the WFS. This also corresponded to the highest value of the FAD Range Weighting within the WFS. A larger maximum FAD angle indicated a higher range of FADs and that was considered a larger functional ability as forces could be applied in a greater variety of directions. This measure does not necessarily relate to strength ability.

2.3 Results

2.3.1 Input and Outcome Measures of the WFS

Hand Dimensions and ROMs

Inputs to the theoretical model and the average data set obtained from human subject testing are shown in Tables 2 and 3. Table 2 shows the theoretical data and the average and standard deviations of the participants' anthropometric hand data while Table 3 shows the maximum and minimum angular measurements. Note in Table 2, the hand dimensions for the theoretical model were generally larger than the average of the experimental data set. In addition, the angular values shown in Table 3 differed between the theoretical and average experimental data for the CMC rotations of the thumb (inclination and azimuth angles) and for the Ab/Ad motions of the fingers. The thumb inclination angle for the theoretical model ranged from 0 to 60 degrees while the experimental data showed average ranges from -15.6 to 27.3 degrees. The thumb azimuth angle for the theoretical model ranged from 0 to 90 degrees, while for the experimental data the average ranged from -6.8 to 36.7 degrees. For the Ab/Ad of the fingers, the theoretical model had a consistent range from -20 to 25 degrees, while the average ranges for the experimental models varied by finger.

Table 2. Hand segment length dimensions: Theoretical data set representing the 50th percentile male and average data for the experimental data (Exp. Avg.) set with nine healthy participants. All values are in mm.

		Distance from Palm Center to CMC		Thumb MC Length	Thumb PP Length	DP Length	DP Thickness
		Lateral	Distal				
Thumb	50^{th} % Male	25.8	-20.0	60.0	21.1	34.4	11.4
	Exp. Avg.	32.0	-36.6	40.0	32.7	27.5	11.4
	Exp. St. Dev.	*4.8*	*7.5*	*3.4*	*2.6*	*2.4*	*1.1*
		Distance from Palm Center to MCP		Fingers PP Length	Finger MP Length	DP Length	DP Thickness
		Lateral	Distal				
Index	50^{th} % Male	25.8	34.4	60.5	22.5	28.4	9.1
	Exp. Avg.	23.1	30.0	44.1	26.8	22.6	9.8
	Exp. St. Dev.	*3.1*	*4.9*	*2.6*	*2.3*	*2.4*	*1.4*
Middle	50^{th} % Male	0.0	42.3	54.6	26.2	28.4	9.2
	Exp. Avg.	0.0	30.8	49.4	30.6	25.5	10.6
	Exp. St. Dev.	*0.0*	*4.3*	*2.3*	*2.8*	*2.8*	*1.4*
Ring	50^{th} % Male	-25.0	35.7	52.8	24.2	29.7	8.5
	Exp. Avg.	-20.2	23.9	44.6	28.0	25.8	10.6
	Exp. St. Dev.	*2.8*	*4.4*	*4.1*	*3.3*	*4.2*	*1.7*
Little	50^{th} % Male	-48.4	31.5	41.4	17.5	27.2	7.8
	Exp. Avg.	-37.4	22.2	36.3	19.7	24.2	9.1
	Exp. St. Dev.	*3.6*	*9.8*	*2.0*	*2.6*	*9.7*	*1.7*

Table 3. Maximum and minimum angular joint values: Theoretical data set representing the 50th percentile male and average data for the experimental data (Exp. Avg.) set with nine healthy participants. All values are in degrees.

		Thumb Inclination		Thumb Azimuth		Thumb MCP Flexion		Thumb IP Flexion	
		Min.	Max.	Min.	Max.	Min.	Max.	Min.	Max.
Thumb	50th % Male	0.0	60.0	0.0	90.0	-10.0	55.0	-15.0	80.0
	Exp. Avg.	-15.6	27.3	-6.8	36.7	-13.3	60.0	-27.6	100.4
	Exp. St. Dev.	*18.0*	*17.5*	*6.1*	*9.3*	*13.7*	*16.2*	*13.4*	*14.1*
		Finger MCP Ab/Ad		**Finger MCP Flexion**		**Finger PIP Flexion**		**Finger DIP Flexion**	
		Min.	Max.	Min.	Max.	Min.	Max.	Min.	Max.
Index	50th % Male	-20.0	25.0	-30.0	90.0	0.0	100.0	0.0	80.0
	Exp. Avg.	-29.1	9.2	-33.3	90.3	-5.9	111.7	-3.6	88.9
	Exp. St. Dev.	*8.3*	*8.1*	*9.6*	*13.4*	*5.7*	*4.8*	*3.1*	*14.7*
Middle	50th % Male	-20.0	25.0	-30.0	90.0	0.0	100.0	0.0	80.0
	Exp. Avg.	-12.8	19.6	-28.4	100.8	-5.8	120.2	-2.1	97.4
	Exp. St. Dev.	*6.0*	*6.6*	*6.4*	*12.2*	*5.5*	*15.3*	*3.5*	*8.9*
Ring	50th % Male	-20.0	25.0	-30.0	90.0	0.0	100.0	0.0	80.0
	Exp. Avg.	-3.9	27.7	-23.3	104.3	-10.1	110.9	-3.2	100.4
	Exp. St. Dev.	*9.3*	*8.3*	*8.0*	*9.8*	*6.4*	*5.3*	*2.5*	*21.0*
Little	50th % Male	-20.0	25.0	-30.0	90.0	0.0	100.0	0.0	80.0
	Exp. Avg.	-7.2	45.2	-29.3	99.3	-13.1	98.7	-5.9	83.1
	Exp. St. Dev.	*6.0*	*10.3*	*15.7*	*9.4*	*14.4*	*6.4*	*8.8*	*26.1*

WFS Model Characteristic Data

The average and standard deviations of the WFS model characteristics of each finger from the individualized WFS models are presented in Table 4. For the fingers, the average experimental values for the amount of reachable volume were all lower than the theoretical values, whereas for the maximum *Number of Ways to Reach* the most accessible point within the WFS, and the maximum orientation angle range at a single point were higher than the theoretical model. However, for the maximum FAD angles, there was a mixture with the little finger experimental data being lower than the theoretical data and the other three sets of experimental data for the index, middle and ring fingers yielding higher experimental values.

Table 4. Characteristics of the resulting FFS model: Theoretical data set representing the 50th percentile male and average data for the experimental data (Exp. Avg.) set with nine healthy participants.

		Volume (cm^3)	Max. Value of # of Ways to Reach the Most Accessible Point	Max. Orientation Angle Range (deg.)	Max. FAD Angle Range (deg.)
Thumb	50^{th} % Male	238.3	48.0	87.8	171.4
	Exp. Avg.	139.8	52.0	64.7	146.8
	Exp. St. Dev.	*56.7*	*21.6*	*13.7*	*16.0*
Index	50^{th} % Male	210.5	238.0	37.5	133.9
	Exp. Avg.	134.4	469.8	52.8	134.7
	Exp. St. Dev.	*33.9*	*72.9*	*2.6*	*8.3*
Middle	50^{th} % Male	199.7	261.0	40.1	125.9
	Exp. Avg.	148.8	447.4	63.0	148.2
	Exp. St. Dev.	*45.8*	*190.8*	*19.5*	*23.3*
Ring	50^{th} % Male	186.8	278.0	37.6	126.1
	Exp. Avg.	110.2	390.8	50.6	133.5
	Exp. St. Dev.	*40.0*	*117.6*	*5.6*	*13.2*
Little	50^{th} % Male	105.8	461.0	37.6	125.6
	Exp. Avg.	100.5	688.9	44.1	110.5
	Exp. St. Dev.	*39.6*	*258.1*	*10.6*	*22.7*

2.3.2 WFS Model Visualizations and Comparisons

Three Dimensional WFS Visualization

The theoretical WFS model of a single finger and the whole hand was also plotted in 3D. Figure 8 shows the entire 3D plot of the FAD weighting parameter for the second digit and the whole hand. In both plots, the blue edge located away from the palm was representative of the points that were reachable by the fingertip, but having only a small range (<30 degrees) of FADs. The red dots indicated the points with high functionality and were located near the palm. Due to the model constraint (Eq. 2) that related Ab/Ad to finger flexion, the WFS produced from the theoretical data set showed a wide splay of reachable points when the finger was allowed Ab/Ad motions at low levels of MCP flexion, but as the flexion of the finger was increased the reachable space narrowed to a plane. In the whole-hand plot, fingers three through five showed similar patterns to the second digit, varying slightly by size and orientation, while the thumb's reachable space and weighting had a distinctly different size and shape in comparison to the fingers. Again, while the blue points were located on the outer edge of the reachable space, the thumb space spanned across the spaces of the other fingers. The same basic 3D pattern was shown for the experimental data.

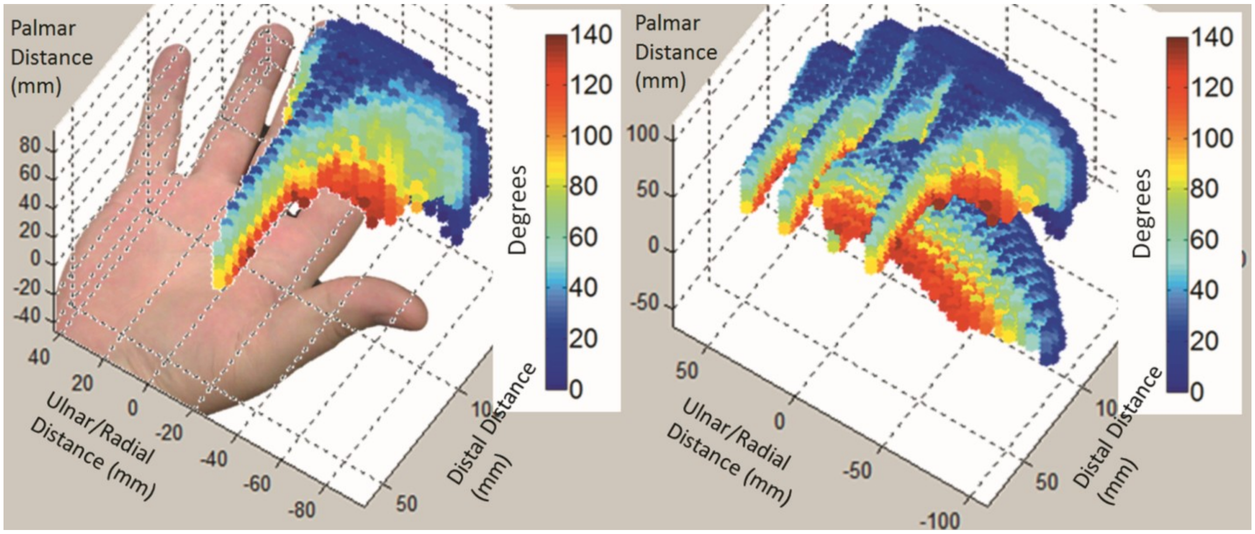

Figure 17. 3D plot of *FAD Range* weighting values for the second digit (left) and the whole hand (right) of the theoretical model. The reachable points for digits two through five all assume a similar shape, while the reachable points for the thumb arc from right to left across the other fingers' reachable spaces.

Visual Comparison of Theoretical and Experimental WFS Models

Sagittal plane slices of the theoretical WFS model and the WFS model from the experimental data of the participant closest to the hand breadth of a 50th percentile hand (88.6 mm for experimental, 90.2 mm for theoretical) are shown in Figures 9-11 for each of the three weighting parameters. Figures 9 and 10 indicated that for both the 50th percentile theoretical model and the closest participant's model the highest levels of functionality for the second digit (determined by *Number of Ways to Reach* each point in space and the ability to orient the fingertip at each point) were in an arc on the interior of the reachable space indicated by the darker red points. The outer edges of the reachable space, indicated in blue, were the areas of least functionality associated with those two weighting methods and were also in good agreement between the theoretical and experimental data set. Figure 11, which was weighted by the ranges of possible FADs, showed that the areas nearest the palm produced largest range of force application directions, indicating that this region had the highest levels of functionality for the second digit when evaluated by force direction and was consistent between the theoretical and experimental data. The areas furthest from the palm showed the lowest levels of functionality as measured by the possible FAD range.

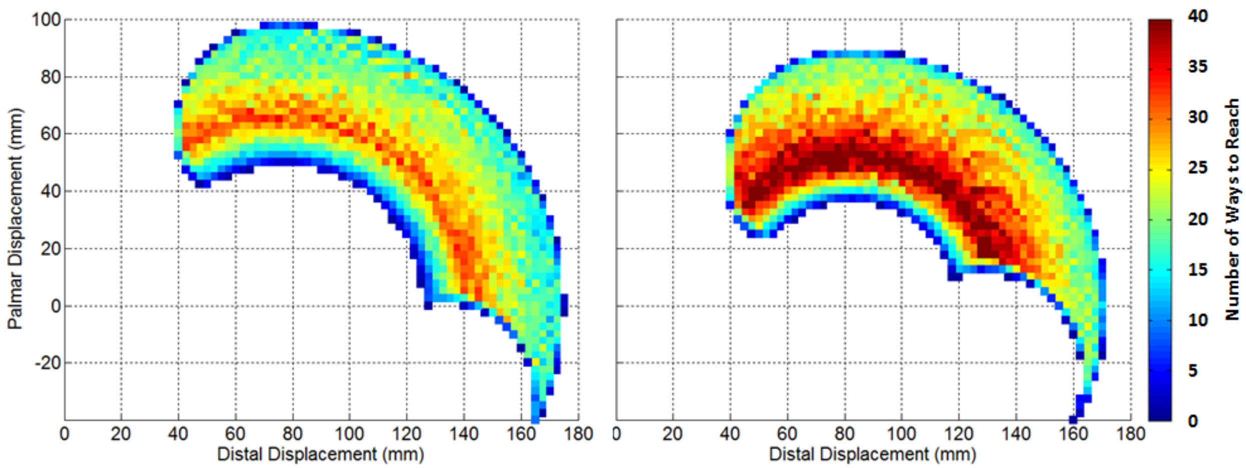

(a) (b)

Figure 18. Sagittal plane plots of the model based on the *Number of Ways to Reach* weighting at each point in the theoretical 50th percentile male WFS model (a) and the WFS model from the experimental data of the participant nearest to a 50th percentile hand size (b). The plots are shown at the level of the second MCP joint. The reachable points are plotted in a color scale where red indicates points in space that are reachable in >30 ways while blue indicates points that are reachable in <10 ways.

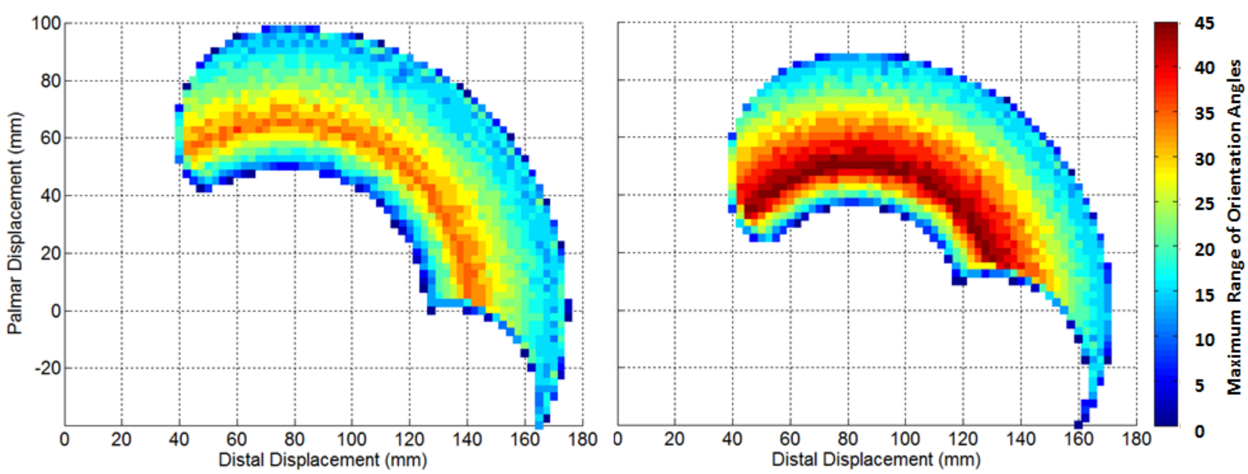

(a) (b)

Figure 19. Sagittal plane plots of the model based on the *Fingertip Orientation Range* weighting at each point in the theoretical 50th percentile male WFS model (a) and the WFS model from the experimental data of the participant nearest to a 50th percentile hand size (b) at the level of the second MCP joint. The reachable points are plotted in a color scale where red indicates points in space that have a range >35 degrees of possible fingertip orientations while blue indicates points that have a range <10 degrees of possible fingertip orientations.

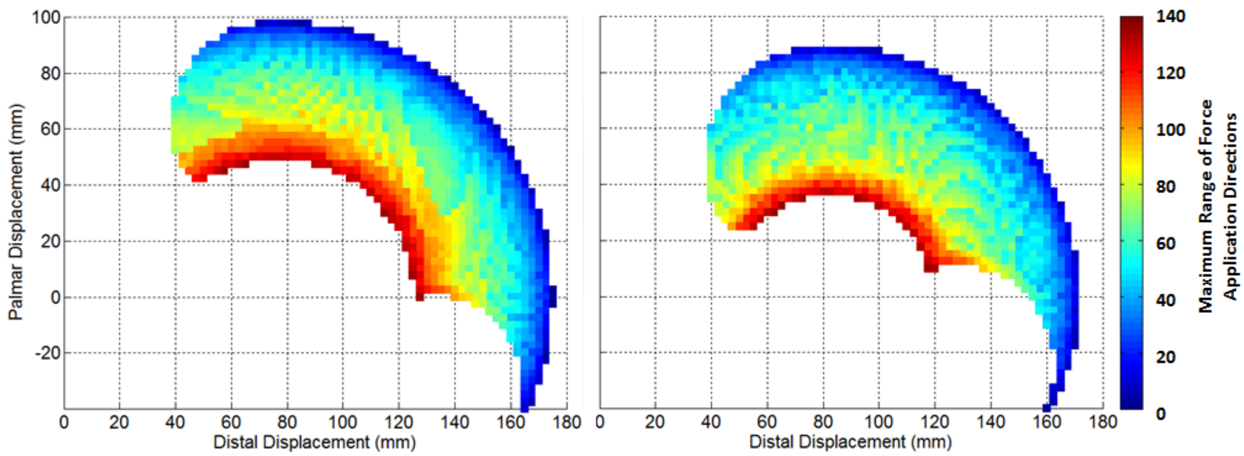

(a) (b)

Figure 20. Sagittal plane plots of the model based on the *FAD Range* weighting at each point in the theoretical 50th percentile male WFS model (a) and the WFS model from the experimental of the participant nearest to a 50th percentile hand size (b) at the level of the second MCP joint. The reachable points are plotted in a color scale where red indicates points in space that have a range >100 degrees of possible FADs while blue indicates points that have a range <40 degrees of possible FADs.

While the theoretical model and the experimental model produced similar plots, there were differences between the two. The theoretical model produced higher palmar displacements and the magnitude between maximum and minimum distal displacement was also larger. This resulted in a "longer and thinner" aspect ratio for the theoretical model while the experimental sagittal plane model was "shorter and fatter". In addition, the experimental model showed higher overall functional values for the weightings in Figures 9 and 10 than the theoretical model.

2.4 Discussion

2.4.1 Comparison of Theoretical and Experimental WFS Data

Fingers

The Ab/Ad angular data in Table 3 showed that for the theoretical model the minimum angles were consistently 20 degrees and maximum angles were 25 degrees for digits two through five, but the experimental models showed variability across the fingers. For the experimental models, the index finger showed larger absolute values for the minimum Ab/Ad angles, while the ring and little fingers showed larger absolute values for the maximum Ab/Ad angles. This finding indicates that a "one size fits all" approximation of the abduction/adduction angles in the theoretical model did not capture the unique abilities of each finger. Therefore, future applications should use Ab/Ad values from experimental data sets, specific to the application.

The summary characteristic data shown in Table 4 indicated that the theoretical values for the volume of reachable points were higher than those shown in the experimental models, matching trends from hand dimensions in Table 2. This is a product of the experimental data deriving from a mixture of females and males, with a variety of hand sizes. The hand sizes of the participants spanned from 2nd to 95th percentile of males, and 2nd to 90th percentile of females, as judged by hand breadth. Average breadth of the experimental data set was of a small male hand (2nd percentile) or a large female hand (75th percentile). The volume of each individual's WFS was dependent on both the hand dimensions and the joint ROMs, but in general, it scaled with the finger dimensions.

Table 4 also showed that the theoretical values of the maximum *Number of Ways to Reach* and maximum orientation angles were lower than the averages of those shown in the experimental models. This resulted from the fact that the number of calculated fingertip positions and orientations was dependent only on the joint ROMs, and not on the hand dimensions. Therefore, for a given number of positions and orientations calculated, a smaller volume of reachable mesh points would yield a higher concentration of positions and orientations at each point. In application, this translates to smaller hands having a higher peak levels of calculated function, but in a smaller space.

Table 4 showed no clear trend in the FAD angle measures between the theoretical and experimental values across all of the fingers. However, it should be noted that while the index, middle and ring fingers displayed slightly higher experimental maximum FAD values than the theoretical values, the little finger displayed lower maximum FAD values than the experimental model. This is likely the result of neglecting inter-finger constraints. Anatomically, the little finger and ring finger are actuated by several of the same muscles, resulting in dependent motions at the joints of those fingers. This finger interdependence is not accounted for in the current iteration of the WFS model, but should be considered for future iterations.

Thumb

The average data sets shown in Tables 3 and 4 indicated differences between the theoretical and the experimental angular values of the inclination and azimuth angles of the thumb. These differences resulted in differences in the two WFS models of the thumb. This was a product of the assumptions made about the theoretical values of the inclination and azimuth angles. Because those measures were a unique nomenclature developed for this research, there were no direct values for the measures available in the literature. Therefore, the theoretical values used were adaptations of the data sets available, chosen to best estimate the actual values. In future work, it will be necessary to collect data to represent these specific measures rather than extrapolating them from the existing data sets.

2.4.2 WFS Visualization Comparisons and Applications

Figures 8-11 all show large amounts of data pertaining to the functional abilities of the hand in a visually accessible format. This color-coded plotting of the WFS data is easily interpreted by a wide range of individuals ranging from engineers to clinicians. Changes in function are garnered when data are gathered and the model plotted across the duration of rehabilitation or pre-/post-surgery. This work promises a means of objectively determining the functional ability of patient hands and outputting results in a meaningful fashion for varied uses ranging from medical to design.

Additionally, determining the most functional reachable point for an individual or group of individuals will depend on the type of task being performed. For example, if the desired task is to be able to touch and orient the fingertip to an object, the *Number of Ways to Reach* and *Fingertip Orientation Range* weighting parameters provide the most salient information to guide design. However, if a range of force directions need to be applied to the object (e.g. to actuate a button), the *FAD Range* weighting would provide more relevant information. In most cases, however, it is anticipated that object design will require an understanding of the all three weightings of the WFS model and they should be used in combination. An example of application could be the placement and orientation of the controls of a motorized wheelchair that need to be placed within the reachable range of fingertips and actuated in directions that the fingers can apply forces.

Comparing the plots of the theoretical and experimental models in Figures 9-11, the same basic color pattern was present in each model, but they were shaped differently. While the theoretical model was a close approximation for an individual person's ability, the "shorter and fatter" aspect ratio of the shape of the reachable point of the theoretical model was not all-encompassing of the characteristics of the closest experimental model, let alone the characteristics that every other individual might possess. In practice, this means that the current theoretical WFS model could be used to guide object design as an estimate of the abilities of an average sized man's hand, but it should not be used as a guarantee that all hands will be able to place and orient their fingertips in the same manner. In the future, this type of variability could be accounted for with: models for both the 50^{th} percentile male and female; error bands to represent population averages; and scalable models developed from a more comprehensive database of experimental hand dimensions and joint ROMs.

2.5 Conclusions

This research developed a model of the human hand capable of calculating and showing all of the possible fingertip positions, orientations and force application directions given dimensions of the hand and ranges of motion at each joint of the fingers. The model was then applied to theoretical data of a 50th percentile male and nine experimentally measured individuals. The experimental data showed that variability exists between the functional abilities of individuals' hands, and that variability can be measured and modeled. The experimental models produced data that indicated generally lower volumes of reachable space but higher levels of functionality when compared to the theoretical model. In addition, the experimental models presented a more finger-specific pattern of Ab/Ad angles than was expected based on the theoretical model.

Comparisons between the 50th percentile theoretical model and the model from experimental data of a similarly-sized hand indicated good agreement. Though much of the data from the 50th percentile theoretical model overlapped visually with the experimental data some differences were identified. Specifically, the theoretical model produced higher palmar displacements and the magnitude between maximum and minimum distal displacement was also larger. Based on the findings of this work, scaling the model to hand size to accommodate functional capabilities of other sized hands should be the next steps in model comparisons.

This approach to hand modeling lends insight for design, rehabilitation, and pre/post-surgical evaluations. Information about the ability of an individual or group of individuals to position, orient, and apply forces through their fingertips provides potential to improve design of handheld objects to accommodate the functional capacities of people afflicted with arthritis or other ailments of the hand, enhancing their quality of life and enabling continued independence through increased ability to perform activities of daily living. Further, the visual nature of the weighted plots of the model has the potential to be used for functional assessment and aid in tracking rehabilitation. The ability to objectively document functional abilities and monitor any changes across the course of treatment or interventions significantly enhances the abilities of therapists and surgeons to provide better informed treatment decisions and care.

2.5.1 Limitations

While this research presents a novel model for evaluation of the capabilities of the human hand, it is acknowledged that the model has limitations. First, the assumption that the palm acts as a single rigid body is simplifying its role in both positioning the fingers and limiting their movement in extreme flexions. It has been shown by El-shennawy et al. that the metacarpals of the hand, particularly the 4^{th} and 5^{th} metacarpals, move independently [32]. Those motions could influence the outcome of the WFS model, potentially increasing the calculated functionality of the 4^{th} and 5^{th} fingers. The metacarpal motions were not included in the current research as it was not feasible to detect the metacarpal movements on living participants, but considerations for these movements will be included for future iterations of the research. Secondly, the calculated abilities of the hand were presented as a best-case scenario, knowing that many other factors could limit the ability to reach and orient the fingertips. Factors such as shoulder, elbow, and wrist orientation affect the hand's ability to actuate the fingers through restricting the muscles, tendons, and nerves that move and control the fingers [33], and any decrease in the ability to control and actuate the hand will result in a decrease in the functional abilities that has yet to be quantified and included in the model. Third, all calculations in the model were made from a purely kinematics perspective, meaning the magnitude of force that can be generated at any particular point in the WFS space is yet to be defined.

3. COMPARISON BETWEEN HEALTHY AND ARTHRITIC HAND FUNCTION USING RANGES OF MOTION AND A WEIGHTED FINGERTIP SPACE MODEL

3.1 Introduction

The ability to detect and quantify changes in hand function is important to patients, therapists, and physicians. Loss of hand function occurs through a myriad of causes and can have a detrimental effect on quality of life and independence [2,4]. In the US alone, arthritis affects over 46 million adults; strokes affect over 7 million adults; carpal tunnel syndrome accounts for over 4 million workers filing claims; and hand injuries are responsible for over 1 million hospital emergency room visits in one year [34–37]. In addition, improvements in hand function occur through surgical intervention and rehabilitation [38,39]. During these changes, comprehensive evaluations of hand function are necessary to grade the amount of function lost or recovered and are an important part of evidence-based medicine.

There are currently two primary ways in which hand function is evaluated in the clinical setting: physical measurements, and questionnaires. Questionnaires rely on an individual self-reporting difficulty with everyday actions performed by the hand and levels of pain in the hand [5,6]. These measurements quantify the functional ability of the hand and are standard practice for clinicians, but rely on subjective feedback from the patient. Physical measurements evaluate quantifiable capabilities such as range of motion (ROM) of fingers' joints, force and torque generation, and the ability to manipulate objects [4,12,40]. These measures provide objective measures, but lack the ability to be transferred to task-based activities. In particular, the ROM measures are limited to single joint values. These values are not evaluated or interpreted in context with the movements of the other joints on that finger or the other fingers, nor can they be used to evaluate the ability to conduct specific tasks such as grasping a toothbrush, or pressing a button on a medication injector. Thus, a gap exists in the ability to take ROM measures from a single joint and combine them with the ROM measures from all other joints in the finger (and the combination of all fingers) into a model that can be used to objectively document and assess changes in overall function of the hand.

The goal of this research was to compare and contrast the functional abilities of healthy individuals with those of arthritic individuals through the use of a new hand model that addresses the gap between ROM measurements and hand function [41]. The Weighted Fingertip Space (WFS) model is a computational model of hand function that translates objective ROM measurements into a 3D representation of hand function weighted in three ways for functional ability: the number of different ways to reach a point in space, the ability to orient the fingertip at each point, and ability to apply force in a range of directions at each point. The findings of this work provide a significant advancement in the ability to assess function of the hand within an individual, for an individual within a given population, and across populations.

3.2 Methods

3.2.1 WFS Overview

The WFS modeling technique is a computational method that uses measures of hand dimensions and ROMs and transforms these measures into a representation of the 3D reachable space of the fingers with three weighting parameters: 1) the number of ways to reach weighting, which represented the number of unique finger postures that had a fingertip position in the localized area of each mesh point, 2) the range of orientation angles, which represented the largest angular range between the orientation vectors that had been collected at each mesh point, and 3) the angle range of possible force application directions (FADs), which represented the largest angular range between the FAD vectors that had been collected at each mesh point. This model has previously been published by the authors [41], but a summary of the model is provided below.

Model Development

The WFS model consists of a cloud of points in 3D space that represent all of the possible points that can be reached by the pads of the fingertips. The reachable spaces are weighted relative the amount of calculated function that each point can represent with a grasping fingertip. In order to calculate all of the possible reachable points and their levels of functionality, several steps were required.

First, the hand was modeled as a linkage system of 16 rigid bodies connected with 15 different joints. Rigid bodies included the palm, first metacarpal, and all of the phalanges. The joints represented were the first carpometacarpal (CMC) joint, the metacarpophalangeal (MCP) joints, and the interphalangeal (IP) joints. The model included a total of 20 rotational degrees of freedom: two rotations about the first CMC joint, abduction/adduction about the second through fifth MCP joints, and flexion/extension about the MCP and IP joints. Model dimensions were based on measurements of participants' hands.

Next, equations for position and orientation of each fingertip based on the rigid link dimensions and the joint angles were developed. For example, for the index finger, a set of equations was developed to calculate fingertip position, and a vector in the normal direction to the fingertip pad surface. These equations were based on the position of the second MCP joint with the respect to the center of the palm and were developed from the lengths of the index finger's proximal, middle, and distal phalanges, and the angles of the MCP, proximal IP, and distal IP joints.

Following the development of the equations, fingertip positions, orientations, and possible force application directions were calculated for all possible finger postures. The finger postures were chosen by determining each unique integer combination of the possible angles within the measured ROMs for that finger. The FADs were calculated at the direction of movement of the fingertip pad if only a single flexion joint of the finger was to be actuated.

Weighting

By rounding the position coordinates to the nearest 2.5 mm value, the resulting collection of calculated fingertip positions, orientations, and FADs were organized to a 3D grid of points. The mesh points were then assigned weighting values based on the three different weighting parameters. Example plots of the FAD weighting are shown in 3D for the index finger and all fingers in Figure 21 with a hand shown for reference.

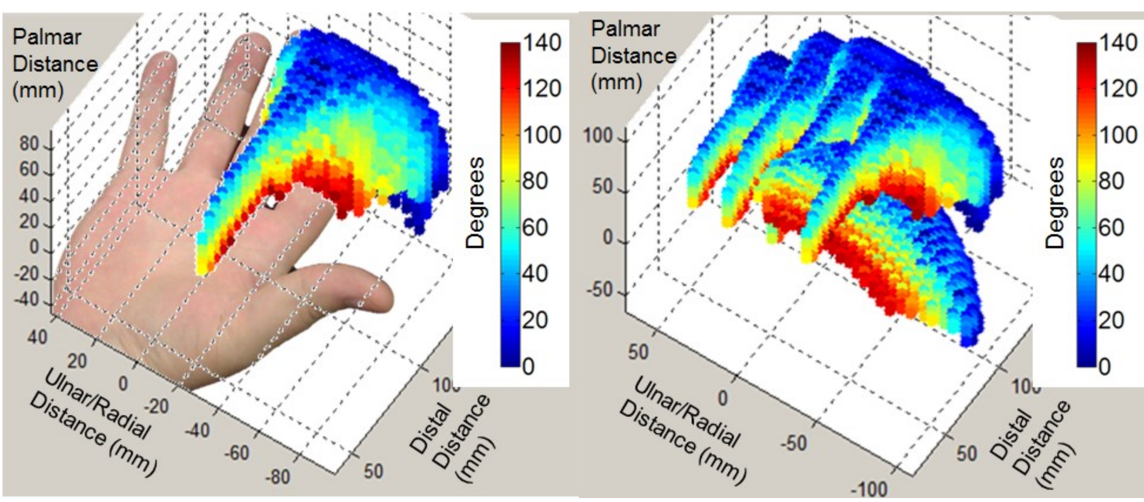

Figure 21. Plot of FAD weighting of the WFS model for an index finger (left) and for the whole hand (right).

Thumb Angle

For clarity in calculation and to avoid redundancy in the description of the movements of the thumb, the motions of the first CMC joint were assigned a spherical coordinate system nomenclature instead of a physiologic nomenclature. The first movement of the CMC joint was described as an inclination angle which represented the angle of the metacarpal away from the centerline of the hand (Figure 22). The second movement of the CMC joint was described as the azimuth angle which represented the amount of rotation of the thumb around the hand. This rotation was measured about the zenith axis, which was a line parallel to the long axis of the hand and through the center of the CMC joint.

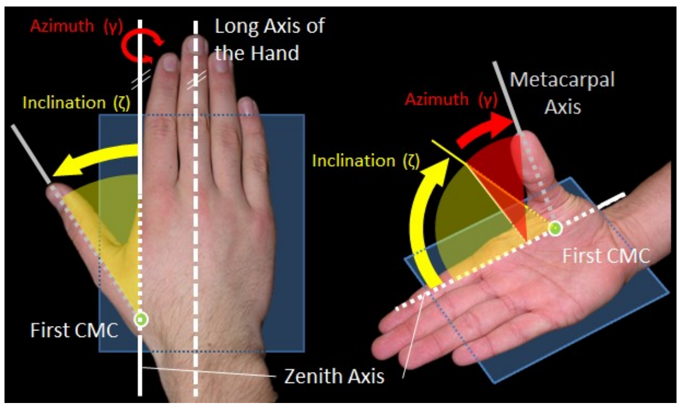

Figure 22. Spherical nomenclature for the movements of the thumb.

3.2.2 Participants

Two groups of participants were included in this research. The first group, the healthy group, consisted of 22 individuals between the ages of 18 and 39 with no reported pain or stiffness in the joints of their hands and no reported injury or disease affecting the hands. The second group, the reduced functionality (RF) group, consisted of 21 individuals who were over the age of 65 and had self-reported a doctor-diagnosed case of arthritis affecting the hand. The healthy group was comprised of 10 females and 12 males, with an average height of 1.73m (SD 0.10 m), average mass of 78.0 kg (SD 18.4 kg), and average hand breadth of 82.98 mm (SD 6.96 mm). The RF group was comprised of 16 females and 5 males with an average height of 1.65 m (SD 0.08 m), average mass of

73.3 kg (SD 13.3 kg), and average hand breadth of 83.52 mm (SD 5.64mm). None of the RF individuals exhibited any noticeable cases of ulnar drift in the fingers, common to individuals with rheumatoid arthritis [42].

3.2.3 Experimental Data Collection

Hand dimensions and finger joint ROMs were necessary for calculation of the WFS model for each individual. The ROMs were gathered using 64 retroreflective markers and a seven-camera motion capture system (Qualisys, Gothenburg Sweden) (Figure 14). With the markers affixed to the hand, each participant moved their fingers through a set of prescribed motions to the best of their abilities to determine the maximum ROM for each motion modeled in the WFS [41]. After the consenting process, participants were asked to complete questionnaires regarding their level of function in their hands. Following that, hand dimensions were measured with a digital caliper (Starrett Model 723).

Figure 23. Marker configuration for motion capture measurements of finger segment movements.

3.2.4 Development of Group Models

For each of the groups (healthy and RF), a group model was developed. The kinematic information from the WFS models of the participants in a given group was combined to produce a single group model. Each group model showed the regions of reachable space that were common to the individuals in that group. To accomplish this, each finger was considered independently, and the 3D WFS model coordinates of each finger were translated so that the MCP joint of that finger was centered at the origin of the 3D space. For example, for the index finger of the healthy group, all 3D WFS models of the index fingers of healthy individuals were translated such that the coordinates of the second MCP joint were at the point x=0, y=0, z=0 in the mesh grid space. Then, each of the mesh points were assigned values corresponding to the number of individuals in the group that could reach that point. A value of one indicated that only one individual in the group could reach the point, while a value of 20 indicated that 20 individuals could reach the point.

3.2.5 Statistical Analysis

T-tests with a significance level of 0.05 were performed for several comparisons (MATLAB version R2013a, Massachusetts, USA). Comparisons were made between the healthy and RF groups for each measured ROM angle (azimuth, inclination, radial deviations, ulnar deviations, flexions, and extensions) for each finger. Comparisons between the females and males within each group were also conducted. In addition, comparisons were made between the healthy and RF groups for the summary values of the WFS models (reachable volume, maximum number of ways to reach, maximum fingertip orientation angle range, and maximum FAD angle range).

3.3 Results

3.3.1 Ranges of Motion

Healthy vs. Reduced Functionality

The summarized ROM values for the healthy group are shown in Tables 5 and 6 for the reduced functionality group. Comparison of the two tables yielded several differences. First, the values of the extension/flexion ranges for the RF group showed lower ROMs than healthy ROMs. This was primarily shown in the flexion angles of the MCP, PIP and DIP angles (as opposed to the extension angles), but the MCP extension angles were also decreased in magnitude. For RF individuals, the average decrease in flexion angles for all of the MCP joints was 5.50 degrees, PIP was 6.88 degrees, and DIP was 19.42 degrees. The average decrease in MCP extension angles for RF individuals in comparison to the healthy group was 15.13 degrees. Statistically, both the MCP extension (index: $p<0.001$; middle: $p<0.001$; ring: $p=0.001$; small: $p=0.004$) and the DIP flexion angles (index: $p<0.001$; middle: $p<0.001$; ring: $p<0.001$; small: $p=0.011$) showed significant differences between the healthy and RF groups for all of the non-thumb fingers. In addition, the index and middle fingers showed significant differences for the flexion at the MCP joint (index: $p=0.005$; middle: $p<0.001$). The thumb showed significant differences in the minimum azimuth angle ($p=0.037$), maximum azimuth angle ($p=0.011$), IP extension ($p=0.022$), and IP flexion angles ($p=0.002$). Lastly, the only radial and ulnar deviations about the MCP joints that were significantly different between healthy and RF populations were for the small finger (radial: $p<0.001$; ulnar: $p=0.043$). All other p-values comparing the angles between healthy and RF groups were greater than 0.05.

Also of note was the PIP extension of the small finger for males in the RF group. It was on average a positive value whereas all other PIP extension values were negative. This was the result of one of the participants having a previous injury that effectively fixed his PIP joint at a positive flexion angle. It affected the mean because of the large value (59 degrees) and the fact that there were only five males in the RF group.

Female vs. Male

Trends between female and male ranges of motion were also identified. Fingers two through five showed similar ROM values for males and females across all fingers and joints for both the healthy and RF groups (Tables 5 and 6). The thumb displayed its own pattern of ROM data. The thumb CMC angles were lower for the males in comparison to the females within both groups, but the overall range was still similar. For example, for the healthy females, the CMC inclination angles ranged on average from -8.8 to 31.40 degrees while the healthy males ranged from -21.75 to 23.75 degrees. The total range of both groups was approximately 40 degrees, but relative to the reference hand position (flat on the table with thumb 45 degrees from long axis of the hand), the values were higher in the positive direction for the females than for the males. The flexion/extension joints of the thumb, MCP and IP angles, were similar across females and males. However, while trends were identified between females and males, the only significant difference shown was for the PIP extension of the small finger of males ($p=0.001$). All other p-values comparing females and males ROMS were greater than 0.05.

Finger Comparison

Several trends were noted across the different fingers of the hands for both the healthy and RF groups in both the female and male participants. First, fingers on the radial side of the hand showed larger radial deviation at the MCP joint while fingers on the ulnar side of the hand showed greater ulnar deviation at the MCP joint. Second, extension values were similar for the MCP, PIP, and DIP joints across fingers two through five. Lastly, flexion values were higher for middle and ring fingers at the MCP, PIP, and DIP joints than for the index and small fingers.

Table 5. Mean healthy range of motion values

		CMC Inclination				CMC Azimuth				MCP				IP			
		Minimum		Maximum		Minimum		Maximum		Extension		Flexion		Extension		Flexion	
		F	M	F	M	F	M	F	M	F	M	F	M	F	M	F	M
Thumb	Angle	-8.80	-21.75	31.40	23.75	-4.00	-15.75	38.90	36.75	-15.30	-12.00	54.40	54.00	-26.70	-33.58	96.00	93.75
	St. Dev.	*9.14*	*19.90*	*5.15*	*23.85*	*11.71*	*10.87*	*15.21*	*11.25*	*12.17*	*15.69*	*14.42*	*15.38*	*9.62*	*11.11*	*13.19*	*16.18*

		MCP Lateral Deviation				MCP				PIP				DIP			
		Radial		Ulnar		Extension		Flexion		Extension		Flexion		Extension		Flexion	
		F	M	F	M	F	M	F	M	F	M	F	M	F	M	F	M
Index	Angle	-25.30	-28.33	13.60	12.67	-34.10	-30.92	89.30	84.00	-7.40	-4.00	110.20	111.50	-4.00	-0.83	85.20	86.25
	St. Dev.	*7.26*	*9.34*	*8.18*	*8.08*	*6.56*	*10.55*	*13.55*	*9.99*	*4.27*	*7.78*	*9.78*	*15.87*	*2.00*	*6.73*	*15.99*	*8.29*
Middle	Angle	-12.70	-11.92	20.00	17.50	-31.80	-26.83	100.10	97.50	-6.20	-2.50	118.70	115.17	-3.20	-3.83	98.80	97.08
	St. Dev.	*5.58*	*4.29*	*5.72*	*5.25*	*6.46*	*11.18*	*12.17*	*7.23*	*3.85*	*9.02*	*10.02*	*13.66*	*3.99*	*5.49*	*14.06*	*16.62*
Ring	Angle	-2.60	-5.50	28.70	22.17	-28.60	-23.25	105.00	103.00	-11.00	-8.50	114.30	116.83	-4.10	-2.58	84.90	95.67
	St. Dev.	*8.64*	*5.60*	*8.19*	*6.78*	*9.65*	*10.48*	*12.21*	*12.05*	*6.91*	*10.72*	*9.29*	*19.84*	*2.77*	*5.57*	*12.30*	*22.61*
Small	Angle	-6.60	-4.17	44.20	42.92	-36.60	-22.33	96.90	95.50	-11.80	-7.67	99.70	97.92	-5.50	-3.67	94.20	83.25
	St. Dev.	*7.47*	*7.71*	*11.02*	*10.18*	*31.39*	*14.79*	*9.98*	*17.25*	*11.06*	*11.47*	*7.57*	*8.83*	*7.98*	*4.27*	*18.83*	*22.70*

Table 6. Mean reduced functionality range of motion values

		CMC Inclination				CMC Azimuth				MCP				IP			
		Minimum		Maximum		Minimum		Maximum		Extension		Flexion		Extension		Flexion	
		F	M	F	M	F	M	F	M	F	M	F	M	F	M	F	M
Thumb	Angle	-10.75	-15.40	23.81	22.80	-2.63	-7.20	27.44	29.40	-12.44	-13.20	54.81	50.60	-19.06	-25.60	79.44	81.60
	St. Dev.	*10.62*	*11.74*	*15.24*	*10.87*	*4.84*	*11.67*	*11.62*	*9.53*	*7.38*	*5.93*	*12.67*	*12.44*	*17.49*	*8.20*	*15.23*	*15.92*

		MCP Lateral Deviation				MCP				PIP				DIP			
		Radial		Ulnar		Extension		Flexion		Extension		Flexion		Extension		Flexion	
		F	M	F	M	F	M	F	M	F	M	F	M	F	M	F	M
Index	Angle	-24.00	-21.80	13.63	16.20	-21.06	-12.60	74.31	78.80	-6.63	-0.60	106.19	106.80	-5.00	-9.00	62.50	72.20
	St. Dev.	*8.91*	*9.39*	*8.55*	*5.45*	*12.07*	*5.98*	*13.85*	*5.59*	*5.50*	*12.42*	*18.31*	*13.81*	*12.46*	*8.72*	*15.11*	*9.65*
Middle	Angle	-9.56	-13.60	18.25	19.20	-18.44	-13.40	87.50	90.40	-9.38	1.60	107.38	115.20	-3.63	-14.80	72.69	84.60
	St. Dev.	*6.85*	*16.53*	*8.27*	*5.50*	*11.57*	*6.31*	*8.67*	*11.52*	*11.36*	*11.72*	*24.06*	*23.17*	*11.31*	*17.51*	*21.76*	*11.10*
Ring	Angle	-2.88	2.40	25.75	22.60	-16.25	-12.80	98.94	101.40	-12.25	-4.80	104.13	109.80	-6.06	-10.00	64.75	64.20
	St. Dev.	*10.33*	*8.62*	*10.55*	*6.54*	*9.61*	*6.53*	*9.52*	*14.47*	*8.98*	*4.92*	*29.36*	*13.24*	*11.69*	*9.27*	*29.60*	*20.18*
Small	Angle	4.06	8.80	51.13	47.60	-11.44	-7.40	95.31	100.60	-12.00	13.60	91.63	88.20	-1.88	-2.80	67.69	81.40
	St. Dev.	*10.92*	*9.91*	*10.71*	*12.66*	*13.02*	*11.74*	*16.21*	*15.71*	*6.01*	*26.02*	*25.13*	*20.80*	*13.00*	*19.61*	*22.70*	*14.06*

3.3.2 Individual Sagittal Plane Weighting Plots

Healthy vs. Reduced Functionality

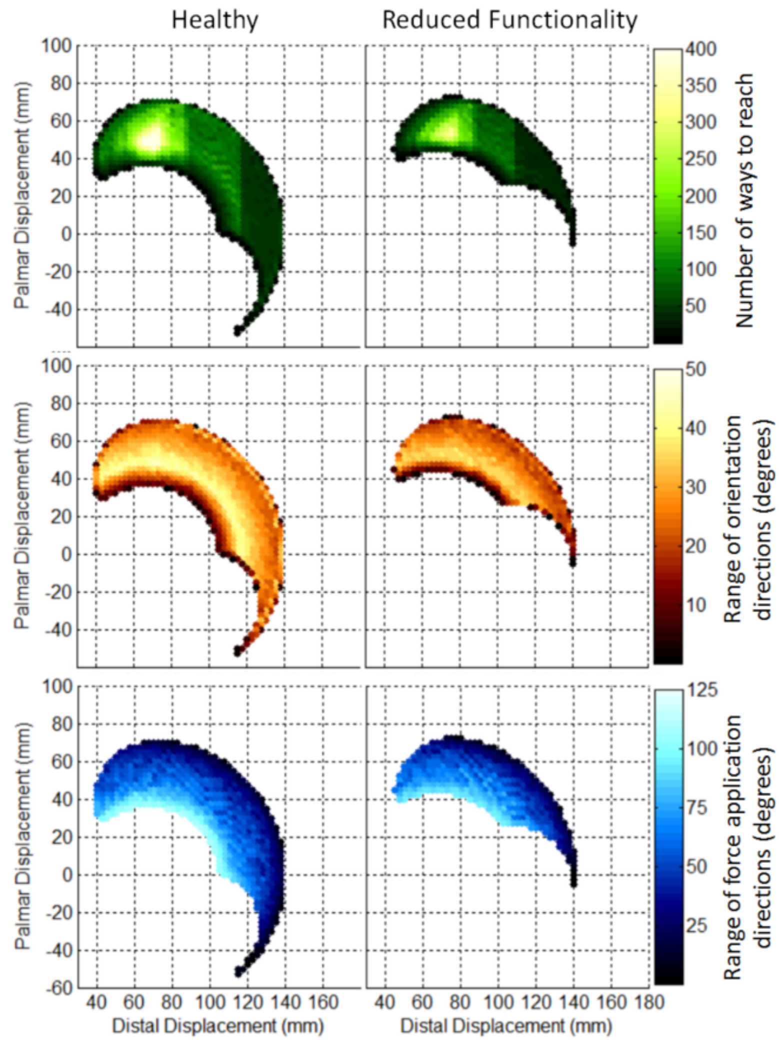

Figure 24. Sagittal plane slices of the three weighting factors of representative healthy (left) and reduced functionality (right) females. The weightings were the number of ways to reach (top), the angular range of possible fingertip orientation directions (middle), and the angular range of possible force application directions (bottom). Darker colors represent lower levels of each functionality measure at the indicated point and lighter colors represent higher levels of functionality.

A 3D version of the WFS model was calculated for every finger of each participant. A sagittal plane slice of the 3D model of the index finger for two size-matched females is shown in Figure 24. The two models are displayed three different ways to indicate the three different weightings: the number of ways to reach each point, the angular range of possible fingertip orientations at each point, and the angular range of possible FADs at each point.

Comparing the plots across the weighting factors yielded similarities between the two groups. First, the pattern for each of the weightings was unique to the weighting, but similar across individuals and groups. For both healthy and RF individuals:

1. The n*umber of ways to reach weighting* indicated the reachable areas with the highest functionality were near the interior of the space, positioned over the center of the MCP joint, Figure 24 (top).
2. The *orientation range weighting* indicated the areas of highest functionality in a band that spanned across the interior of entire reachable range with the points of lowest functionality where the fingers were either spread away from the palm or clenched tight, Figure 24 (middle).
3. The *FAD range weighting* indicated the areas of highest functionality nearest the palm where the fingers would be clenched, and the lowest functionality at the reachable points furthest away from the palm where the fingers would be outstretched, Figure 24 (bottom).

Second, while the size and scales of weightings changed slightly with each individual, the general shape of the reachable space was similar for each of the fingers. As seen in each of the plots in Figure 24, the reachable space was a band of points in roughly a semi-circle centered about the MCP joint.

Comparing the plots across the healthy and RF groups showed several differences as well. First, the reachable points showed higher levels of functionality across all three measures in the healthy participants when compared to the RF participants, as indicated by the lighter-colored points in the representative plots on the left in Figure 24. Second, there tended to be more reachable points in a wider and longer band for the healthy participants than for the RF participants.

Female vs. Male

Representative sagittal plane plots for a healthy and a RF male are shown in Figure 25. When compared to Figure 24, these plots show some of the differences between the female and male WFS models. The most notable differences are the overall size of the reachable space and the scale of for the *number of ways to reach weighting*. The females showed, in general, smaller reachable volumes and higher number of ways to reach a single point, while the males showed larger reachable volumes and lower numbers of ways to reach a point. These trends held true across both healthy and RF groups.

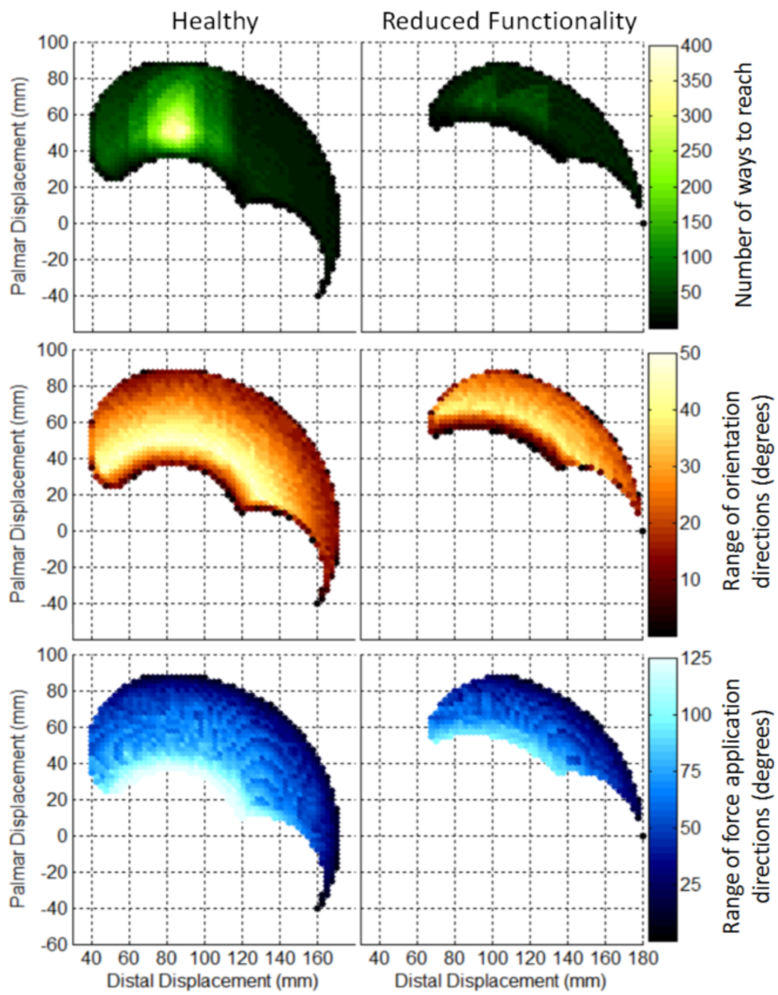

Figure 25. Sagittal plane slices of the three weighting factors of representative healthy (left) and reduced functionality (right) males. The weightings were the number of ways to reach (top), the angular range of possible fingertip orientation directions (middle), and the angular range of possible force application directions (bottom).

Summary of Groups with Table

The trends seen visually in the representative sagittal plane plots were also evident across the entire sample of participants. The average values of the reachable volume and maximum values of the three functional weightings for the healthy and RF groups are presented in Table 7 and Table 8. These data quantify the trends of the maximum functional values across the groups (healthy vs. RF and female vs. male) as well as across the fingers.

When comparing the healthy and RF groups, trends showed that the maximum functional values for each of the three weightings and total *volume of reachable space* were lower for the RF group except for the *numbers of ways to reach* measure for the males' thumbs. Differences were statistically significant for all volume measurements (thumb: p=0.003; index: p=0.008; middle: p=0.003; ring: p=0.011; small: p=0.002), for the thumb for all measures (*number of ways*: p=0.014; *orientation range*: p=0.012; *FAD range*: p=0.018), for the index finger *number of ways to reach* measure (p=0.020), and for the ring finger *FAD angle range* measure (p=0.025).

As shown in the plots, when comparing healthy females and males, females were able to reach smaller volume, but tended to have larger number ways to reach each point, while maximum orientation angle ranges and FAD angle ranges were similar across females and males. The trends of female to male comparison held true when comparing the RF population except for *FAD angle range*, where RF males showed higher maximum values than RF females.

Tables 7 and 8 also provided a means to compare the different fingers of the hand. The thumb showed high volumes of reachable space, but lower maximum *number of ways to reach* values in comparison to the other fingers. Next, of the other fingers, the index and middle fingers showed largest reachable volumes of digits two through five. For example, for the healthy females, the average reachable volume for the index and middle fingers was 116.53 cm^3 and 133.93 cm^3, respectively, while the ring finger reached on average 97.97 cm^3 and the small finger 85.26 cm^3. Lastly, the maximum orientation angle range and FAD range were similar for the index, middle, and ring fingers, but lower for the small finger. These trends held true for both healthy and RF populations and across both females and males.

Table 7. Summary values of the WFS output parameters for healthy subjects.

		Volume (cm^3)		Max. Value of # of Ways to Reach		Max. Orientation Angle Range (deg.)		Max. FAD Angle Range (deg.)	
		Female	Male	Female	Male	Female	Male	Female	Male
Thumb	Mean	115.00	170.01	67.00	44.00	59.18	65.07	137.91	135.53
	St. Dev.	*55.32*	*79.29*	*29.01*	*10.86*	*10.51*	*20.94*	*19.41*	*15.78*
Index	Mean	116.53	145.73	499.60	486.58	52.79	52.08	131.66	135.87
	St. Dev.	*23.26*	*66.80*	*81.25*	*314.11*	*5.69*	*11.04*	*12.60*	*23.83*
Middle	Mean	133.93	140.67	466.40	322.83	59.94	57.92	147.51	139.58
	St. Dev.	*42.04*	*41.06*	*117.94*	*151.98*	*11.55*	*16.25*	*17.32*	*22.09*
Ring	Mean	97.97	113.46	484.60	489.83	54.96	61.31	137.29	135.57
	St. Dev.	*29.38*	*46.47*	*190.36*	*505.51*	*5.65*	*34.26*	*12.91*	*20.14*
Small	Mean	85.26	94.28	829.40	549.67	46.59	42.67	117.00	107.18
	St. Dev.	*37.47*	*50.66*	*178.80*	*230.77*	*7.84*	*7.34*	*12.83*	*21.03*

Table 8. Summary values of the WFS output parameters for reduced functionality subjects.

		Volume (cm^3)		Max. Value of # of Ways to Reach		Max. Orientation Angle Range (deg.)		Max. FAD Angle Range (deg.)	
		Female	Male	Female	Male	Female	Male	Female	Male
Thumb	Mean	77.93	113.47	103.81	57.40	49.78	48.01	123.27	121.08
	St. Dev.	*41.42*	*26.58*	*71.59*	*10.69*	*16.54*	*11.83*	*18.82*	*23.52*
Index	Mean	88.06	99.40	359.44	332.60	50.41	53.01	118.91	127.66
	St. Dev.	*45.78*	*44.63*	*129.08*	*134.02*	*12.84*	*7.29*	*27.73*	*18.02*
Middle	Mean	77.66	130.68	333.63	422.80	49.98	61.24	122.21	140.81
	St. Dev.	*35.09*	*91.67*	*209.44*	*448.72*	*16.14*	*22.44*	*41.21*	*30.27*
Ring	Mean	73.41	66.86	383.75	225.00	52.06	50.15	113.19	118.92
	St. Dev.	*47.76*	*39.70*	*241.22*	*134.95*	*21.16*	*11.89*	*43.98*	*28.49*
Small	Mean	52.55	46.84	608.31	420.40	44.24	40.13	104.11	99.00
	St. Dev.	*32.89*	*34.61*	*327.08*	*308.20*	*12.19*	*7.78*	*34.97*	*24.49*

3.3.3 Group Three Dimensional Plots

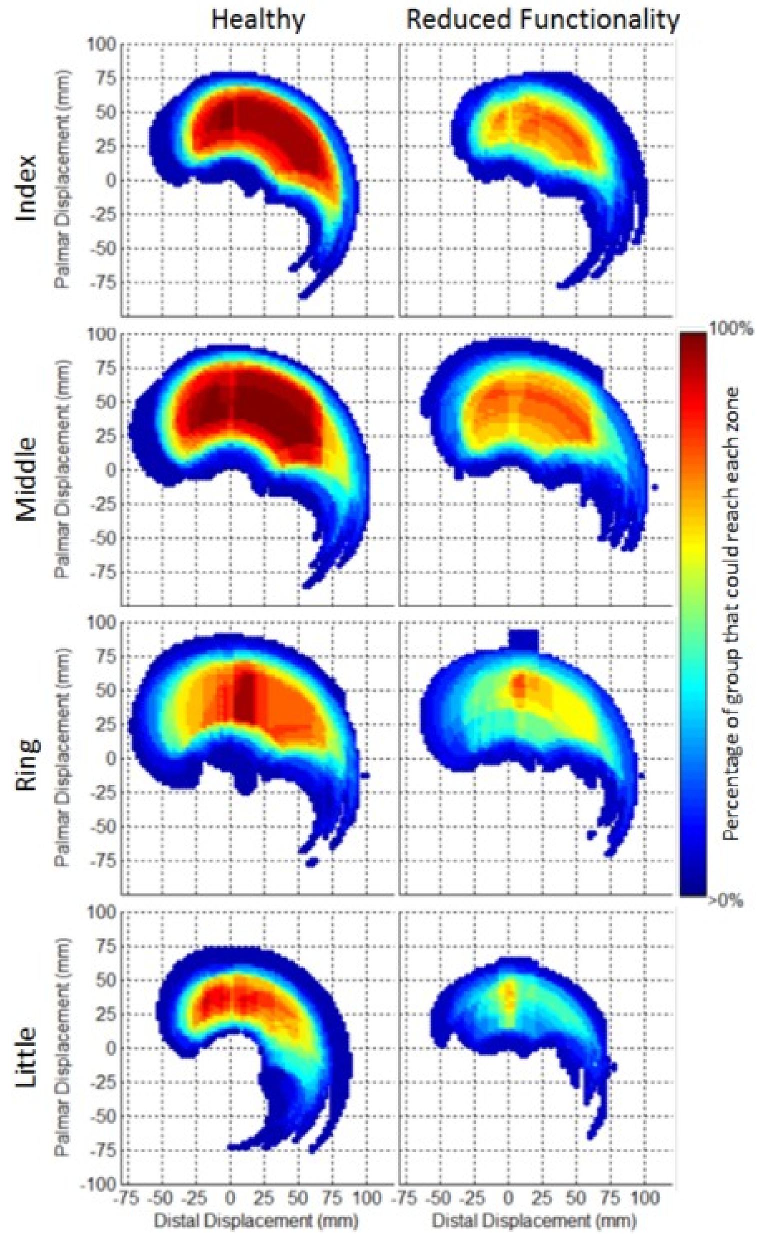

Figure 26. Planar slices of 3D reachable space for healthy (left) and reduced functionality (right), for the index (top), middle, ring, and small (bottom) fingers. Color weighting values indicate number of sample population that could reach each point in space with dark red indicating 100% of the participants reaching that zone, and dark blue representing that only one participant could reach that zone.

Sagittal plane slices of the combined group 3D plots are shown in Figure 26 for the healthy and RF groups. The index, middle, ring and small fingers are shown with the colors representing the number of individuals in each group that were able to reach that point in space. Dark red points indicated areas in space where all of the individuals were able to reach while dark blue indicated areas where only a few of the individuals could reach. All 22 healthy participants were able to reach at least a subset of the same zones for all fingers while the RF group was not. Only 18 out of 21 participants for the RF group were able to reach overlapping zones for the index and middle fingers.

Comparisons of the fingers using the planar slices yielded several results. First, when evaluating the shape and pattern of the overlapping areas, the areas in space of highest overlapping values were the same for the healthy and RF participants. For every finger, this was located in the interior of the band of reachable space. Secondly, for both the healthy and RF groups, the middle finger had the largest zone of overlapping ranges, followed by the index finger, then ring, then small.

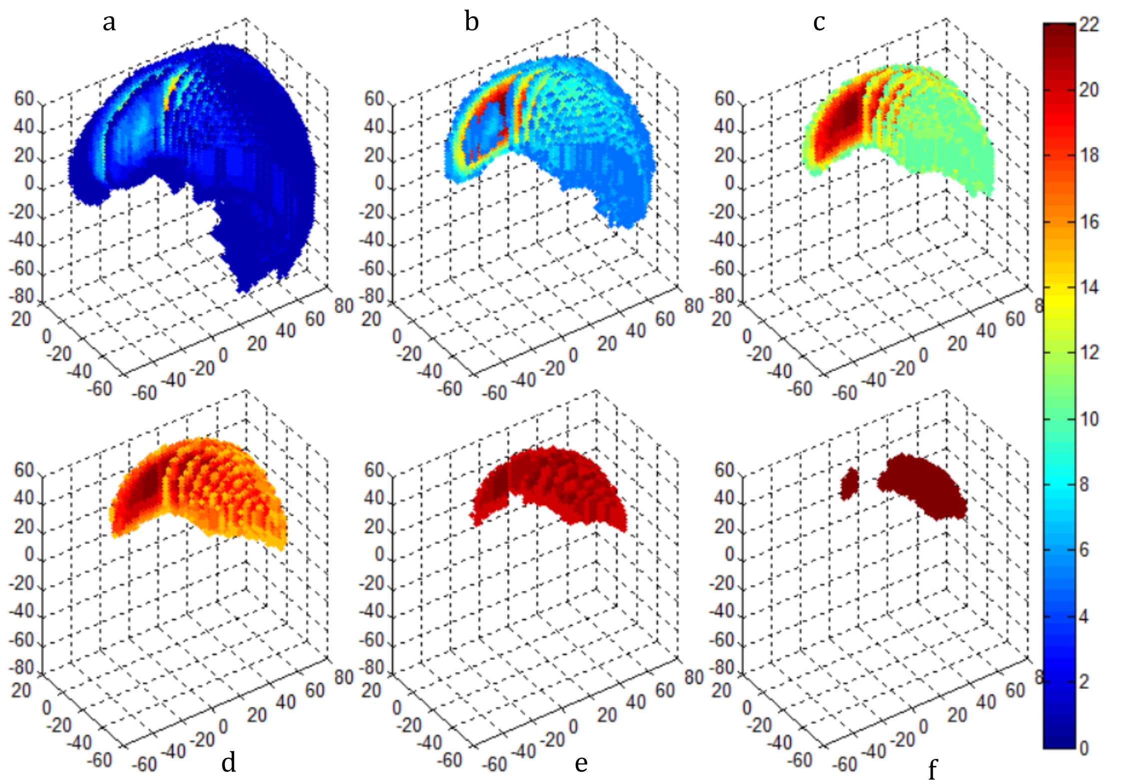

Figure 27. Three dimensional views of the overlapping reachable spaces for the index finger of the healthy population. From top left to bottom right: (a) all reachable points, (b) points reachable by at least five individuals, (c) reachable by at least ten individuals, (d) reachable by at least 15 individuals, (e) reachable by at least 20 individuals, and (f) reachable by all individuals.

The full 3D representation of the healthy group's overlapping WFS model for the index finger is shown in Figure 27. The same model is shown in six different plots that represent the shape of the reachable space. The general shape was widened when the finger was near extension (on the right of each plot) and nearly planar when the finger was flexed (on the left of each plot). When viewed as a progression of least to most reachable (a to f), the layers of the 3D group model peel back to reveal the most universally reachable spaces in the middle of the volume. The blue areas on the outside of the model are only reachable by a few of the individuals in the group, but the red areas that are left in the middle are reachable by most or all of the individuals in the group. The same general pattern was shown for the RF group, as plotted in Figure 28.

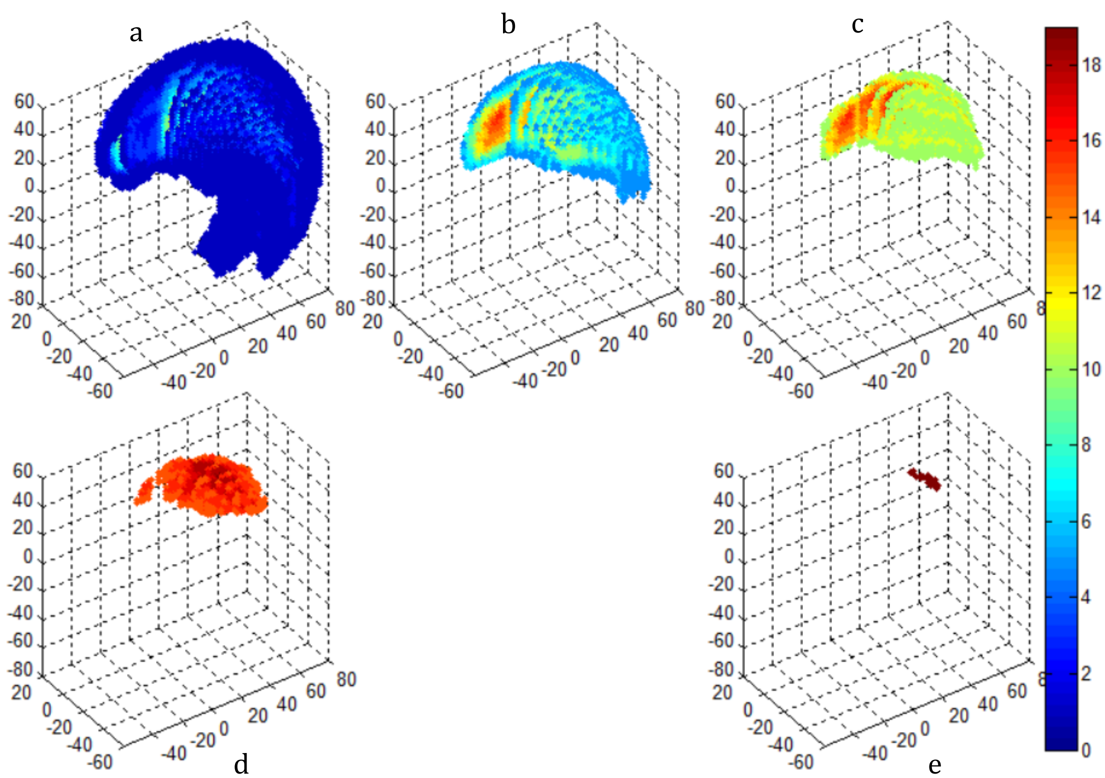

Figure 28. Three dimensional views of the overlapping reachable spaces for the index finger of the RF population. From top left to bottom right: (a) all reachable points, (b) points reachable by at least 5 individuals, (c) reachable by at least 10 individuals, (d) reachable by at least 15 individuals, (e) reachable by at least 18 individuals (the maximum out of 21 total in group).

Comparison of the healthy and RF group models, shown in Figures 18 and 19, revealed many of the same trends visible in the sagittal plane plots. That is to say the healthy group model reaches a slightly larger but similar space as the RF group model, and the region of most reachable points on the interior is larger for the healthy group model. Also visible was that there were no spaces that all of the RF participants could reach.

3.4 Discussion

This research compared and contrasted the functional abilities of healthy individuals with those of arthritic individuals through the use of the WFS model. ROM data, qualitative sagittal plane plots, quantitative values of the 3D plots, and group models were compared.

3.4.1 Ranges of Motion

Deviations in radial and ulnar angles between the healthy and RF groups were not significant for the index, middle and ring fingers. Thus, the ability to move those fingers side-to-side does not appear to be affected by arthritis. For hand evaluation purposes, these data suggest that a 3D model of the functional finger space will not need to include abduction and adduction of the fingers for an evaluation of functionality. The majority of the differences in ROM values were in the flexion and extension angles and the functional changes in flexion and extension were seen in sagittal plane models. The removal of the abduction and adduction components from the model could have several benefits. For example, calculating WFS models of only the sagittal plane drastically reduces computation time in comparison to the full 3D models. Next, the sagittal plane models can be shown and interpreted a 2D format, making them more accessible in print medium as opposed to needing a 3D visualization tool for interpretation. Also, when considering the use of the WFS models in a clinical environment, this would reduce the number of measures needed to produce a model.

Based on this information, it is possible that lateral motions could be used more frequently than they currently are in activities of daily living. However, the ability to move the fingers laterally is limited as the fingers are flexed at the MCP joint. This means that for the full range of lateral motion to be achieved, the MCP joints must be flat with the palm. Also, as lateral movements are not commonly used to manipulate objects, the coordination and strength of these movements is not anticipated to be high. Because of these constraints, using lateral movements would only be recommended for tasks and objects requiring low force magnitudes such as sliding switches or swiping a touchscreen but nonetheless provides a basis for consideration of alternative movements.

Another finding in the ROM results was the unequal centering of the radial and ulnar deviations in the fingers. Previously reported findings of radial and ulnar ROM at the MCP joints all showed a uniform distribution across the fingers or showed only a single value for ROM [22,43]. In the current research, this resulted because the fingers were being obstructed in adduction by the other fingers. For example, the index finger was able to move laterally in the radial direction limited only by the physical structure of the index finger, but in movements toward the ulnar direction, the finger was limited by contact with the middle finger. On the ulnar side of the hand the opposite was true, where the small finger was relatively unobstructed in the ulnar direction, but came into contact with the ring finger in the radial direction. While specific care was given to choose finger motions that would elicit the maximum range of measurable lateral movements, it is possible that the greater adduction ranges could be achieved if the fingers were allowed to overlap. These were not included in the current research for several reasons: first, was that these overlapping motions are rarely used in daily activities and second was that it was not possible to measure given the marker configuration on the posterior of the fingers. It is believed that the extended range of adduction from these motions would be negligible, but future research should be conducted with this focus.

3.4.2 Individual Sagittal Plane Weighting Plots

Qualitative Comparison

Visual comparison of the healthy and RF sagittal plane plots yielded differences that can be used in evaluating hand function. By viewing the WFS plots it is possible to see that the plots from healthy individuals showed longer and thicker bands of reachable space with more areas of high functionality than the plots from RF individuals. The fact that the healthy individuals showed higher levels of functionality was not revolutionary, as the groups were chosen to have differing levels of functionality, but rather that the size, shape, and patterns of highest functionality could be shown in a way that could be understood with a quick visual inspection. This type of information can be helpful in evaluation of function of the hand in either a clinical setting or for design of objects with respect to the hand. Particular to the clinical environment, it may be possible for the planar plots to be developed from goniometric measurements of the flexion and extension angles, and provide the clinician with a greater understanding of the level of function while adding minimal time to the patient/clinician interaction.

The patterns produced by each weighting were consistent across the individuals, regardless of the level of functionality or the size of the hands. Therefore the weighting patterns were linked to the structure of the fingers and the allowable ROMs at the joints. For example, the areas of reachable space with the highest values for the *FAD range* weighting were always nearest the palm, as seen in Figure 24 (e) and (f). The ability to reach those areas was dependent on the finger's ability to flex the PIP and DIP joints, meaning that as the ability to move those joints decreases, the ability to reach the zones of maximum FAD range will decrease for any individual.

The three weighting factors of the WFS models each produced a unique pattern that was consistent across the healthy and RF groups, however, the patterns were distinct from one weighting to another. This indicated that a given fingertip position may fall in a high-function region for one weighting but lower-function region for another weighting. For example, a task that requires a large range of force applications direction may be best achieved with the finger clenched tight and fingertip positioned near the palm, but that fingertip position would be poor for fingertip orientation possibilities.

Given the three different weighting patterns, it would be expected that the fingertip positioning with the reachable space would correspond with the type of weighting that was most needed for a given task. For example, grasping tasks that require a large amount of finger dexterity or various different ways to grasp an object would be guided by the *number of ways to reach* weighting pattern and result in finger placements in the small zone on the interior of the reachable space. Similarly, grasping tasks that would require a range of fingertip orientations, such as writing, would be guided by the *range of orientation angles* weighting and fingertip positions would be chosen in the band of high values through the middle of the space. Lastly, grasping tasks that require holding onto an object that is applying different directional forces, such as holding a toothbrush, would utilize finger positions in the zones of high *FAD range* weighting, nearest the palm. This understanding could be used in future research to examine the influence of the weighting and task on finger posture and fingertip placement.

Quantitative Comparison

The observations made qualitatively were supported by the quantitative values calculated in the model. In comparison to the healthy group, the WFS models of the RF group showed lower values for *volume of reachable space*, *maximum number of ways to reach*, *maximum orientation angle*, and *maximum FAD angle* across the fingers. While all of the fingers showed decreases in average values for the RF group, the thumb showed significant differences for every functional measure. This indicated that the model was able to quantify differences in maximum potential function of the hands and that for the test population the thumb was the most affected finger.

When used as a tool for evaluation of functional capacity, the results showed that the WFS model had interdependent relationships that should be accounted for. First, the volume of reachable space was approximately proportional to hand size. While the ROMs for the genders were approximately the same, the smaller hands of the females were calculated to reach smaller volumes. In addition, while the females were able to reach smaller volumes, they also had larger maximum *numbers ways to reach* values. The number of calculated finger postures in the WFS model is dependent only on the ROMs. Therefore, given equal number of calculated finger postures, a smaller hand would be expected to exhibit a more condensed collection of reachable points in a smaller volume. Consequently, the measures of *volume of reachable space* and *number of ways to* *reach* were inversely proportional to each other. This means that if using *volume of reachable space* or the *number of ways to reach* weighting as a measure of comparison, only individuals of similar hand sizes or the same individual at different times should be compared.

In contrast, the maximum *orientation angle range* weighting and maximum *FAD angle range* weighting were similar across females and males. Differences in hand sizes had little to no influence on the ability to orient the fingertip and apply forces in a range of directions. Instead, the orientation angle and FAD angles were dependent primarily on the ROMs and independent of hand size, and can be used as comparison measures regardless of whether the individuals being compared.

Second, when comparing the different fingers of the hand, the thumb should be evaluated independent of the other fingers. This is because the structure and allowable motions differ from the other fingers. From the results, the thumb showed higher volume of reachable space, but lower maximum *number of ways to reach* values in comparison to the other fingers.

The WFS models were not normalized based on hand size. This decision was made so that the calculated space of reachable areas corresponded to the specific individuals. For comparisons between a person's abilities at different times (e.g. pre/post-surgery) a normalization is not necessary. However, the use of a WFS model with a normalized hand size could provide a broadly applicable model for comparison to the general population. Future work will evaluate normalization of the WFS models.

3.4.3 Group Comparison Plots

The sagittal plane group plots showed that for the healthy group, a "universal space" existed that could be reached by all individuals. The exact same cannot be said for the RF group, as not all individuals were able to reach the same spaces, but spaces did exist where all but three individuals could reach. Further, the areas of highest overlapping values for the RF group were the same areas as the healthy. Therefore, when evaluating an individual's hand for the level of functionality, the healthy or RF group WFS model can be used as a guide to show what areas the individual can reach with respect to other similar individuals or the healthy population sample. In addition, this knowledge can be beneficial when choosing intervention strategies for rehabilitation. The universal space can be used as a guide during rehabilitation to indicate which spaces the rehabilitation should focus on regaining. Further, tasks and objects can be developed that utilize this space, ensuring the largest number of individuals will be able to accomplish the task or hold the object.

3.4.4 WFS Limitations

While the WFS modeling method provided a unique pathway to understand the spatial relationship of the functionality of the hand, limitations to the model still exist. First, treating the palm as a single rigid body underestimates the movement capability of the metacarpals of the hand [32]. Second, the ROMs used for input to the model were measured while the rest of the upper extremity was positioned comfortably, allowing for maximum ROM to be measured. It has been shown that elbow and wrist positions have an effect on the ability to control and actuate the hand [44], so using the finger ROM at comfortable wrist and elbow positions produced WFS models that represented a "best-case" scenario that may not be representative of all arm postures. The effect of these limitations on the current research was considered negligible on the basis that the effects would be equal on all individuals.

It should also be noted that while individuals with arthritis were recruited for this research, no major ailments or deformities of the hand were present in the tested participants that were outside the modeling assumptions of the hand. This is important to note because deformities such as ulnar drift would be inconsistent with the assumptions of the model, and the resulting WFS would not be representative of the actual space that was reachable by the individual. For evaluation of the WFS model for hand deformities inconsistent with the underlying hand assumptions, a specific version of the equations for position and orientation would need to be developed or additional constraints added to the ROMs.

3.5 Conclusions

In conclusion, the ROM data, individual WFS models, and group models all showed results that can provide a better understanding of the three dimensional changes in functional abilities of the hand. The ROM data showed that differences and similarities existed between the ROMs of the healthy group and the RF group. The differences in ROM were primarily in reductions of flexion/extension angles for the RF group, meaning that 2D plots should be sufficient for evaluation of change. In addition, no differences were noted between groups in abduction/adduction angles for the index, middle and ring fingers, so those motions should be implemented in activities of daily living where possible. For both groups, no differences were found between females and males except for those that were attributed to differences in hand sizes.

The WFS data indicated that the decreased ROM for the RF group when compared to the healthy group translated to decreased calculated functionality. Qualitatively, decreased functionality in the RF group was shown by the size, shape, and weighting patterns of the 2D and 3D plots, so using the WFS models to qualitatively assess the functionality of the hand will provide an understanding of the spatial relationships of the functionality in the measured hand that are unavailable elsewhere. Quantitatively, the difference between the healthy and RF groups was shown by the lower functional values for reachable volume, maximum number of ways to reach, maximum range of orientation angles, and maximum range of FAD angles. This was interpreted to mean that the WFS models can be used to quantitatively detect changes in functionality of the hand. In addition, hand size should always be considered when using the WFS as an evaluation tool as hand size had an influence on the volume of reachable space and the *number of ways to reach* weighting. Therefore, size-matched hands should be used to draw conclusions from comparisons of the reachable volume or *number of ways to reach*.

The combined group models showed that a universally reachable space existed. All individuals in the healthy group were able to reach a subspace of overlapping points. Not all individuals were able to reach the same spaces for the RF group, but there were areas where all but three individuals could reach and those areas were in the same spatial locations as the areas of highest overlap for the healthy group.

In total, the WFS model provides a novel tool that can detect and display differences in hand function with objective kinematic-based values. Therefore, this model has the potential to guide clinical decisions, quantitatively document treatment effects and surgical interventions, and identify changes during rehabilitation. The development of this tool will strengthen clinical care by facilitating evidence-based medicine.

4. MAPPING KINEMATIC FUNCTIONAL ABILITIES OF THE HAND TO 3D OBJECTS FOR INFORMED DESIGN OF HANDHELD DEVICES FOR HEALTHY AND ARTHRITIC POPULATIONS

4.1 Introduction

The ability to perform many of the activities during daily living is dependent on the hand's functional ability to grasp and manipulate handheld objects. Individuals are living longer and increased age has been shown to correlate with losses in the ability to use the hand [12]. In addition, ailments such as arthritis, stroke, carpal tunnel syndrome, and hand injury each adversely affect hand function on a daily basis for millions of individuals [34–37]. These ailments result in decreases in joint ROM and decreases in the ability to generate forces with the hand [10]. These decreases have been shown to lead to limited abilities to perform activities of daily living [4] and, consequently, decreased independence [2]. In order to maintain the ability to manipulate objects as functional ability is lost, either the individuals need to adapt and use different strategies to accomplish these tasks, or the object being manipulated must be designed to match the abilities of the person.

As such, there is a need to understand the interface interactions between the hand and the object. Several models have been developed that define the abilities of the hand in terms of reaching three dimensional (3D) spaces [18,19,29,45] and have the potential to quantify hand object interactions. The weighted fingertip space (WFS) model is one such model that calculates the reachable spaces and the only model that weights the spaces according to functional abilities [41]. These weightings address the fingers' abilities to reach a point, the angular range of possible fingertip positions available at a given point, and the directions in which forces can be applied to an object with the fingertip. Yet, a need still exists for translating the 3D kinematic abilities of the hand into a design space and applying them to device development. Specifically, there is a need to show that information about the functional abilities of hands can be translated to design of handheld objects for populations with reduced functionality (eg. arthritis, stroke).

Therefore, the goal of this research was to show that mapping the WFS to object designs can be used to objectively determine the design that best matches the functional abilities of an individual or groups individuals. Matching the object design to the hand’s abilities has the potential to improve device design so that independence will be increased through increased ability of the users to manipulate objects needed for everyday life.

4.2 Methods

4.2.1 WFS Modeling

The framework for evaluating and modeling functional hand capabilities used in this research was the WFS model previously developed by the authors [41]. The WFS model is a 3D point cloud representing the points that are reachable by each fingertip in space and weighted by the levels of functionality available to the fingertips at each point. The functionality is weighted by three separate parameters:

1) The *number of ways to reach* weighting represented the relative number of possible finger postures that allow a fingertip to reach each point.
2) The *range of orientation angles* weighting represented the angular range of possible orientations that the fingertip could assume at each point.
3) The *force application direction (FAD) range* weighting represented the angular range of possible directions the fingertip could apply forces at each point.

The WFS model for each individual was developed in the same way. First, the hand was modeled as a system of 16 different rigid bodies, corresponding to each of the phalanges of the hand, the first metacarpal and the palm. The rigid bodies were connected with 15 different joints, capable of producing 20 unique angular rotations, corresponding to flexions/extensions and abductions/adductions of the fingers, and flexions/extensions and rotations of the thumb about the carpometacarpal joint. The lengths of each of the bodies were measured for each individual using a caliper. The ROM for each angular rotation was determined using motion capture measurements made while the individuals performed prescribed hand motions designed to illicit the full ROM at each joint. The rigid body model of the hand was then used to calculate equations for the fingertip position and orientation for each finger with respect to the palm as functions of the joint angles. Fingertip positions, orientation vectors, and possible force application direction vectors were calculated for all joint angle combinations feasible within each finger's ROMs. The volume of reachable points was then organized to a mesh grid of points and the grid points were weighted based on the three functional parameters. An example of the WFS model for the index through little fingers of the hand is shown in Figure 29.

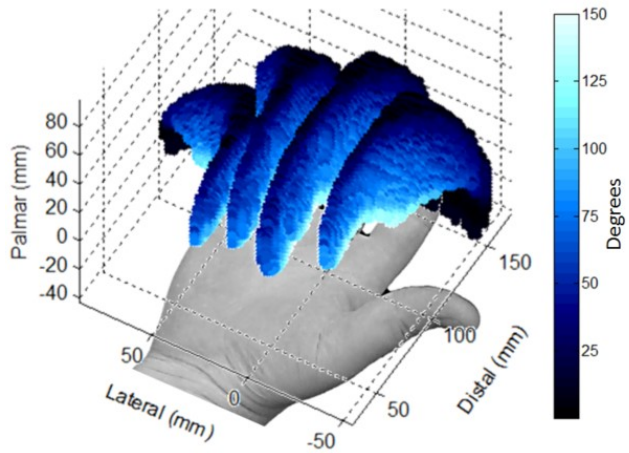

Figure 29. Three dimensional representation of the WFS model showing the *FAD range* weighting for the index through little fingers with respect to the orientation of the hand

The WFS models were calculated using experimentally measured hand dimensions and calculated finger joint ROMs. The ROMs were calculated from 3D motion capture measurements using 64 markers on the posterior of the hand.

4.2.2 Development of Group WFS Models

Group WFS models were calculated by merging the WFS models from several individuals. The healthy group model was developed from the measurements made on 10 women and 12 men between the ages of 18 and 39 without any reported injury or difficulty using their hands. The reduced functionality (RF) group model was developed from the measurements made on 16 women and 5 men that were over the age of 65 and self-reported a case of doctor-diagnosed arthritis. The healthy group had an average hand breadth of 82.98 mm (SD 6.96 mm), and the RF group had an average hand breadth of 83.52 mm (SD 5.64mm).

The group models represented the number of the participants out of each group that could reach the same points in 3D space. This was calculated by first determining the average position of each MCP joint of the individuals in each group. Then the WFS models for each finger were translated such that the individual MCP location was moved to the group-average MCP location. Finally, each point in a Cartesian mesh grid spaced at every 2.5mm was weighted by the number of individuals from the group that were able to reach each point.

4.2.3 Auto-injector

The auto-injector was the object chosen for design evaluation with the WFS models. Auto-injectors are cylindrical handheld devices that are commonly used by patients to self-inject medicines such as epinephrine and arthritis medications. Operation of the auto-injector is performed by grasping the device in one hand, holding one end of the cylinder against the skin, and then pressing a button to inject the medication into the skin. The auto-injector was chosen for the sample object in this research because it is a simply-modeled cylindrical object that is commonly held and actuated with a single hand by people with varying ranges of functionality in their hands. Three commercially available auto-injectors are shown in Figure 30.

Figure 30. Three commercially available auto-injectors. Note the auto-injectors vary in diameter and button placement.

The cylinder was modeled in Matlab as a surface mesh of discretized points for evaluation using the WFS model. The interface surface was modeled as a curved side surface of a cylinder. The cylinder had a length and similar to a common auto-injection device, 160mm. Five different diameters were used for the cylinder, ranging from 20mm to 60mm in increments of 10mm, to encompass the range of diameters in the commercially available auto-injectors as well as diameters outside the commercial range. The cylinder model was positioned in the 3D space of the WFS model with its long axis parallel to the line between the second and fifth MCP joints, anterior to the MCP joints the distance of the MCP thickness, with end of the cylinder protruding 25mm beyond the breadth of the hand in radial direction. The surfaces of the cylinder model were discretized to a mesh of points spaced approximately 2.5mm apart. The cylinder models were simplified further for the purposes of evaluating cylinder diameters in a power grasp, a grasp that involves wrapping the index through little fingers around an object laid across the hand and squeezing the object between the fingers and the palm. To avoid including points that would be physically reachable by the fingers, but not feasible for holding the cylinder against the palm (i.e. points facing the palm), only mesh points on the top half of the cylinder (furthest from the palm) were included, Figure 31.

4.2.4 Mapping the WFS to the Object

The individual WFS models were mapped to the surface mesh points of the cylinder to determine where and how each fingertip could interact with the cylinder surface. For both the individual WFS model and the group models, this was achieved by determining the WFS point closest to each surface mesh point and assigning the WFS weighting values to that surface point. A visual representation of this process is shown in Figure 31. The top plot shows the FAD weighting of the WFS model of the index finger in color in a sagittal plane with the cross section of the cylinder in black. The bottom plots shows the WFS weighting values mapped to the surface mesh points of the cylinder cross section.

The mapping of the WFS onto the cylinder was evaluated using the index through little fingers of the WFS models. The thumb was excluded during this analysis as the thumb pad is not used in a power grasp, but rather is used to actuate the firing of the device.

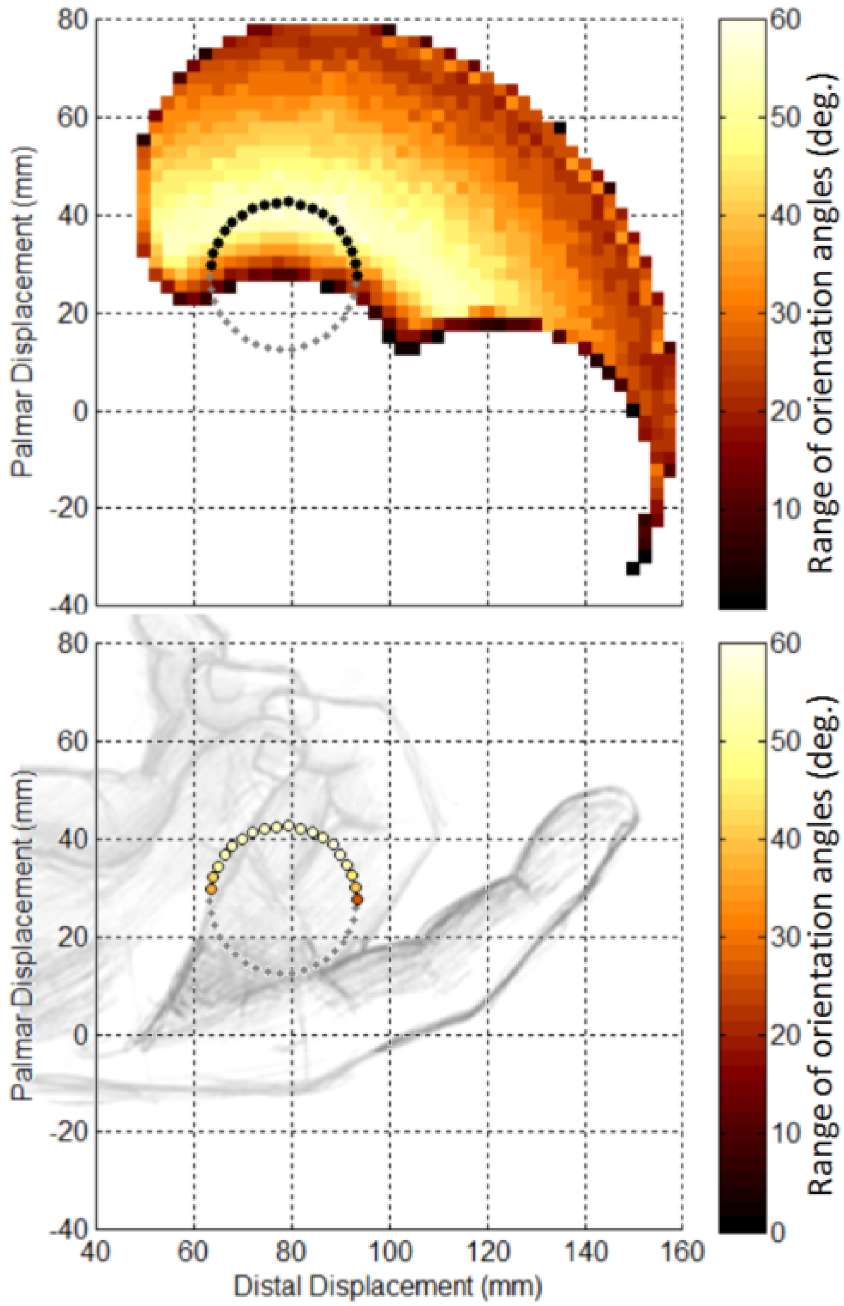

Figure 31. Sagittal plane view of the WFS model and the cylinder profile points in black. Solid gray dots indicate the bottom half of the cylinder where WFS points were not mapped (Top) The WFS model is shown for the *FAD range* weighting with dark orange representing low angular ranges and the lighter yellows representing high angular ranges. (Bottom) WFS values mapped to the surface points of the cylinder model with hand shown for reference

4.2.5 Design Variation and Analysis

Individual WFS Models

The WFS model was mapped to the surface of the cylinders 20, 30, 40, 50, and 60 mm in diameter for all individuals. Each cylinder diameter was evaluated qualitatively and quantitatively using four different measures: the total amount area that the fingertips could potentially reach on the surface of the cylinder, the *number of ways to reach* weighting, the *range of orientation angles* weighting, and the *FAD range* weighting.

Patterns of highest and lowest functionality for each weighting parameter were identified, as well at the shape and size of reachable areas. These patterns were identified within a single cylinder diameter across the different weighting parameters. In addition, how each weighting pattern changed across the range of different diameters was identified.

Quantitatively, the WFS model mappings were summarized using the maximum weighting values and the total reachable areas for each finger. Single values were used to represent each finger because for a single grasp of an object, each finger will only occupy one position on the surface. The maximum values were chosen to indicate the highest potential level of function that was available for surface interaction. To summarize the entire ability of the hand to interact with the surface of the cylinder, the maximum weighting values of each of the four fingers were summed into a single value for the hand.

These evaluations were performed for all 43 participants. An example of a single representative participant was developed for presentation of the qualitative analysis. The quantitative analysis included average and standard error calculations of the maximum weighting values for each group and the total reachable areas of each group.

Group WFS Models

The two group models were also mapped to the five cylinder models to analyze how universally reachable each diameter was for the groups. Because the weighting of the group models represented the number of individuals in each group that could reach the same points in space, the mappings of the group models represented the number of individuals from each group that could reach the same areas on the surface of the cylinders. The number of mapped points to the surface of each cylinder were summed and multiplied by the area each point represented (6.25 mm^2) to indicate the total amount of reachable area for each percentage of the group. The data for points reachable by at least 50% and 75% of the groups were included for both the healthy and RF groups. In addition, the data for points reachable by at least 90% and all individuals were included for the healthy group.

4.3 Results

4.3.1 Mapping the WFS to Auto-injector

Figure 32 shows a healthy participant's WFS model mapped to a 30 mm diameter cylinder for all three weighting parameters. This model was chosen because it was representative of the healthy group models. The weightings each mapped to the cylinder in unique ways. The *number of ways to reach* weighting mapped the highest values to the top of the cylinder positioned furthest away from the palm for each finger. The *range of orientation angles* weighting plotted similarly with the areas of highest functionality away from the palm, but in a broader band of points across the top surface. In addition, the *range of orientation angles* weighting showed the highest values occurred for the index and middle fingers. The *FAD range* weighting showed highest levels of functional mapping on the side of the cylinder for each the fingers.

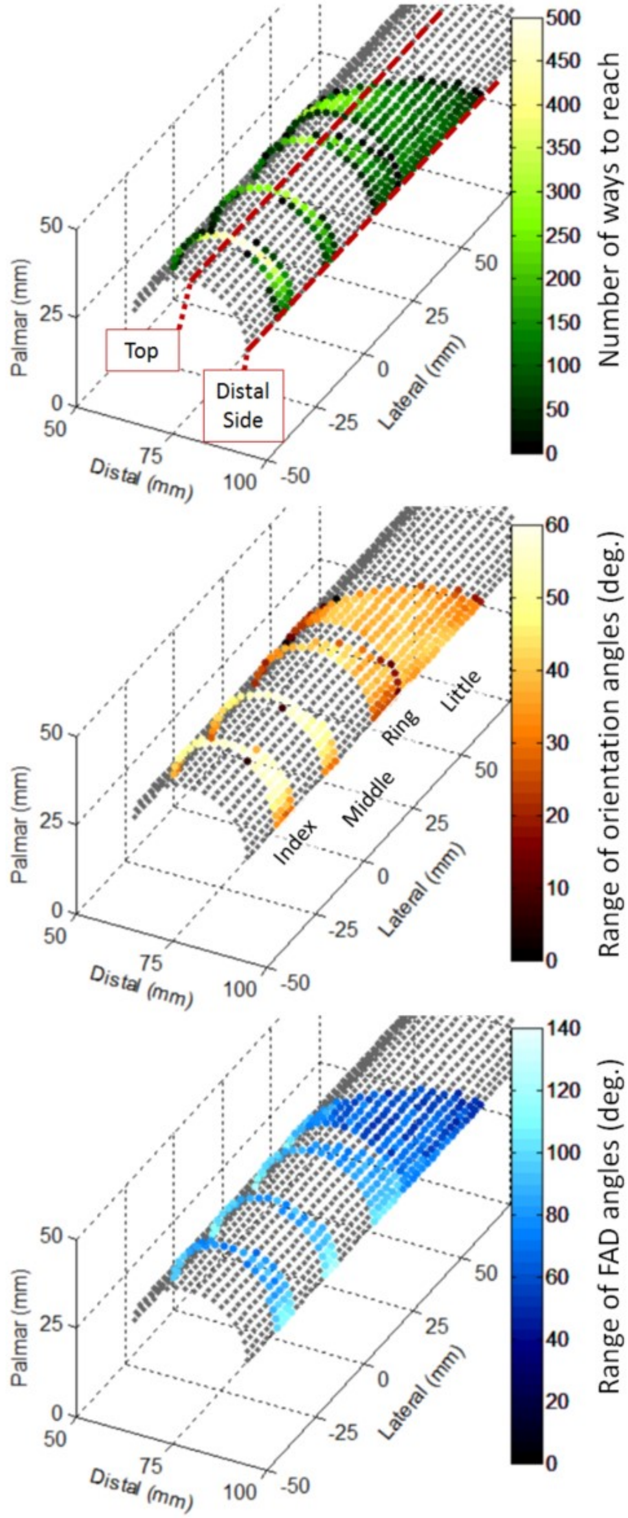

Figure 32. Three weightings of the WFS model of a single participant mapped to the surface points of the cylinder. (Top) The *number of ways to reach* weighting is plotted in shades of green with regions of the cylinder labeled. (Middle) The *range of orientation angles* weighting is plotted in shades of red and orange with the mappings labeled by finger. (Bottom) The *range of FAD angles* weighting is plotted in blue. For all weightings, darker colors represent lower levels of functionality, while lighter colors represent higher levels of functionality

4.3.2 Design Variation with WFS Model

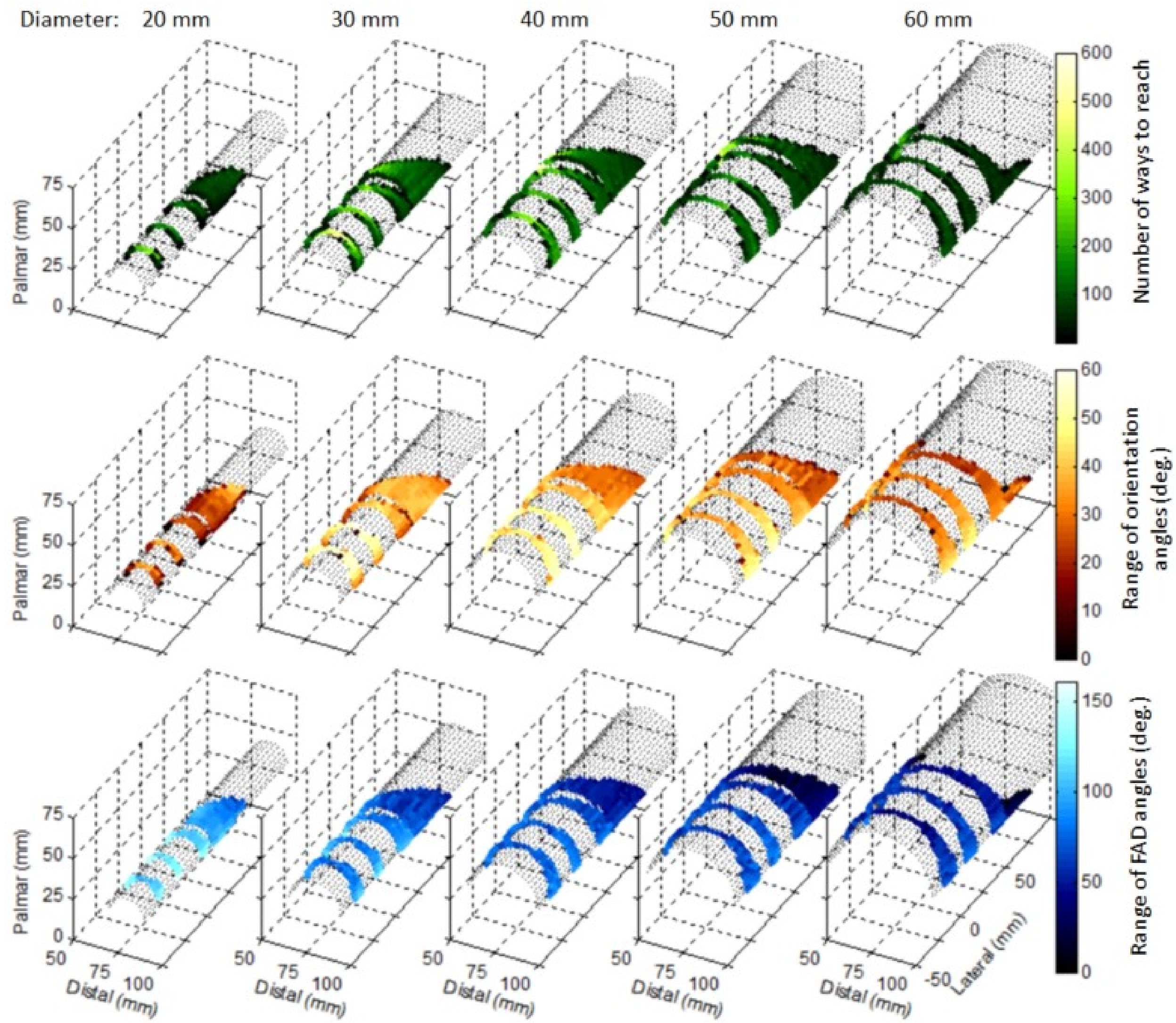

Figure 33. The three weighting parameter of the WFS model plotted to half cylinders of dimensions ranging from 20-60 mm in diameter.

The weightings of the WFS model for the same representative participant are shown in Figure 33 with the weightings mapped for diameters of 20, 30, 40, 50, and 60 mm. For the *number of ways to reach* weighting, the reachable area on the surface cylinder with the highest functional value was consistently positioned on the top of the cylinder, regardless of the diameter. For the *range of orientation angles* weighting, the area of highest functional weighting value changed from being the top of the cylinder for the smaller cylinders (20 and 30 mm) to the distal and proximal sides of the cylinder for the larger cylinders (50 and 60 mm). The *FAD range* weighting showed the highest functional values on the distal and proximal sides of the cylinder consistently across the diameters, but with decreasing total magnitude of the weighting with increasing cylinder size.

The maximum weighting values were calculated for each finger at each diameter, then the values were summed to represent the maximum potential functional capacity of the hand for each diameter, and a summary of the values is shown in Figure 34. The average summed values are shown for the healthy and RF groups, with the error bars indicating the standard error for each data point.

The healthy group showed two different optimal diameters for the three functional weighting parameters. The *number of ways to reach* weighting and the *orientation range* weighting both indicated the 40 mm diameter was the cylinder with the highest average cumulative functional weighting. The *FAD range* weighting indicated the 30 mm diameter cylinder had the highest functional weighting. The 40 mm diameter showed the second highest value for the *FAD range* weighting.

The RF group showed three different optimal diameters based on the different weightings. The *number of ways to reach* weighting showed the highest average functional weighting at for the 30 mm cylinder. The *orientation range* weighting indicated the 50 mm cylinder had the highest weighting, and the *FAD range* weighting indicated the 40 mm cylinder as best. Both the *number of ways to reach* and the *range of orientation angles* weightings showed 40mm as producing the second highest mapped weighting values.

Comparing the healthy and RF weighting data showed that the two groups followed similar trends, but in general the RF values were lower than the healthy values. The only exceptions to this were the *number of ways to reach* weighting and the *orientation range* weighting at 20 mm.

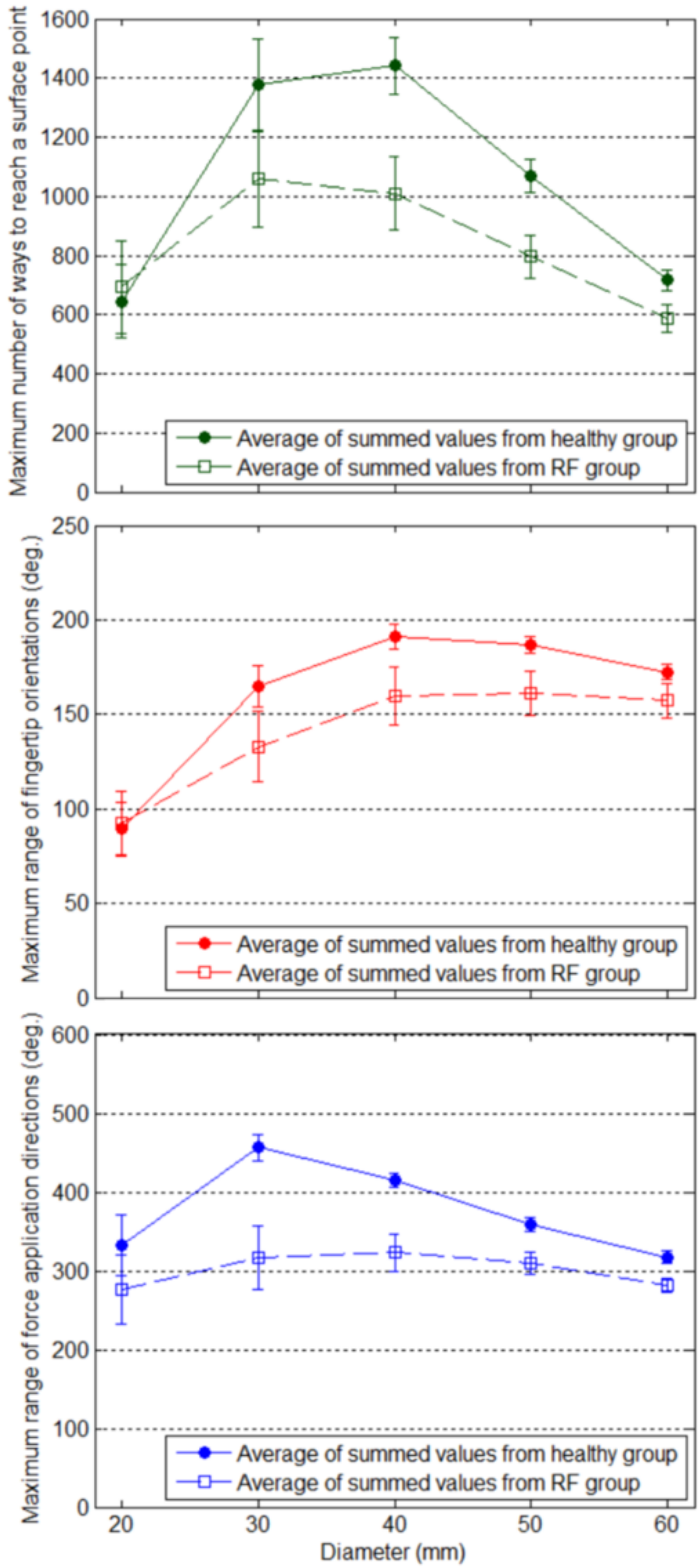

Figure 34. Summary values of the maximum WFS weightings mapped to the surface of the cylinder plotted by diameter. Values represent the sum of the weightings from all four fingers. Standard error is shown in the error bars for the healthy and RF groups. (Top) *Number of ways to reach* weighting (Middle) *Range of orientation angles* weighting (Bottom) *FAD range* weighting.

The total potentially reachable area for each participant was also calculated for all four fingers for each cylinder diameter. The average and standard error values for the two groups are shown in Figure 35 for each diameter. The healthy and RF groups both showed a trend of increasing values of reachable area with increasing diameter.

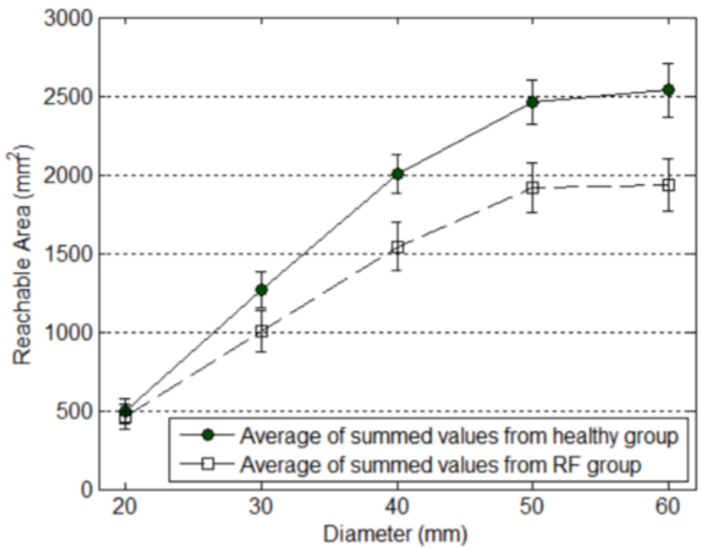

Figure 35. Summary of the total reachable area for each diameter cylinder

4.3.3 Universal Design using the Group Models

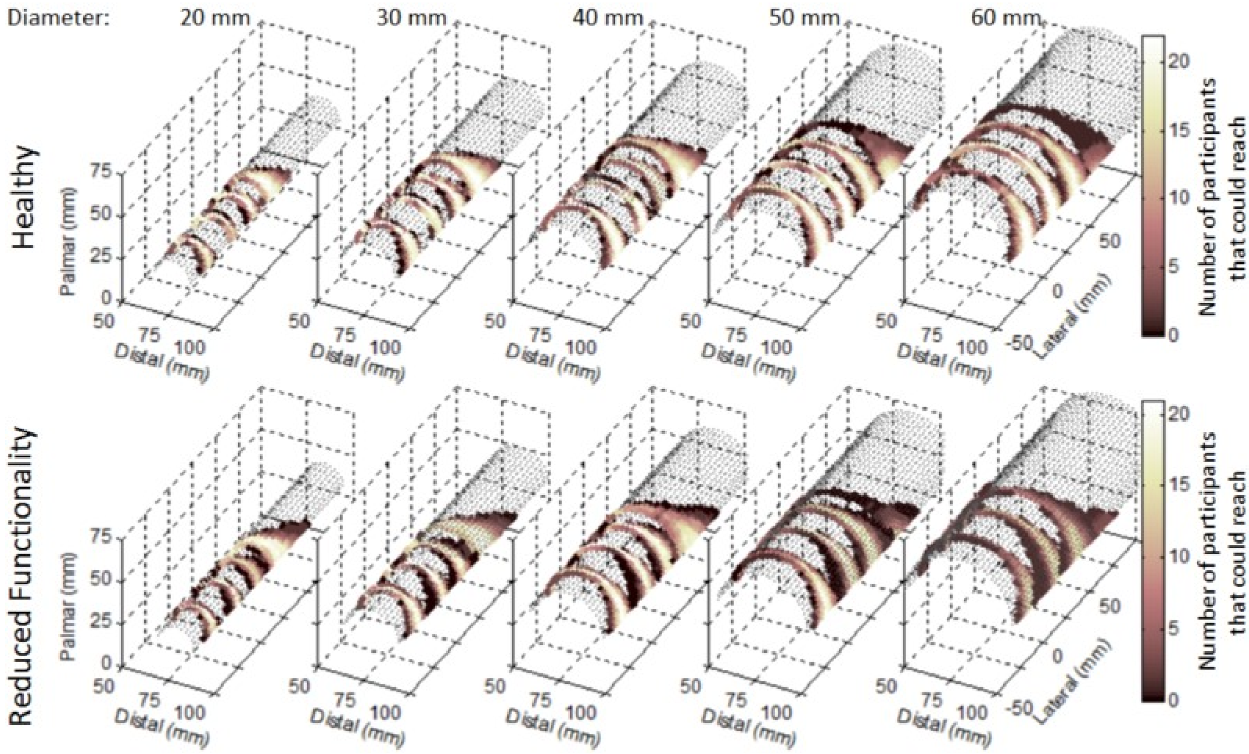

Figure 36. Group WFS models plotted to the surface of half cylinders positioned for a power grasp. Darker colors indicate a small percentage of the group was able to reach each point while lighter colors indicate a higher percentage of the group was able to reach. (Top) Healthy group model (Bottom) Reduced functionality group model

The mappings of the group models to the surface of the cylinder models are shown in Figure 36. Spatially, the data showed that the little finger was the finger least able to reach the top of the larger cylinders for both groups, based on the dark colors and absence of colored points. Comparing the two groups, at least one person from the healthy group was able to reach the top of the cylinder with all four fingers, while no participants from the RF group were able to reach the top with the little finger for the 60 mm diameter. For each finger, the areas of most reachable points were near the centerline of the finger, and areas where few individuals were able to reach were oriented lateral to the centerline of the fingers.

Figure 37 shows the summary values of the group models. The cylinders were each analyzed with respect to the percentage of each group that could reach the cylinder surface. The values were plotted with respect to the amount of overall area that each percentage of the group could reach on each cylinder with all four fingers. The data showed that for the healthy group, the diameter that was most reachable by all of the participants was 40 mm. However, the most reachable cylinder if only 50% of the healthy group was required to reach the surface was at 50 mm. For the RF group, no diameters were reachable by all or even 90% of the group. The highest percentage of the RF group that was able to reach the same points was 86% (18 of 21 participants) on areas the 50 mm and 60 mm cylinders. For at least 50% and at least 75% of the RF group to be able to reach the surface of the cylinder, the 40 mm cylinder showed the highest reachable area.

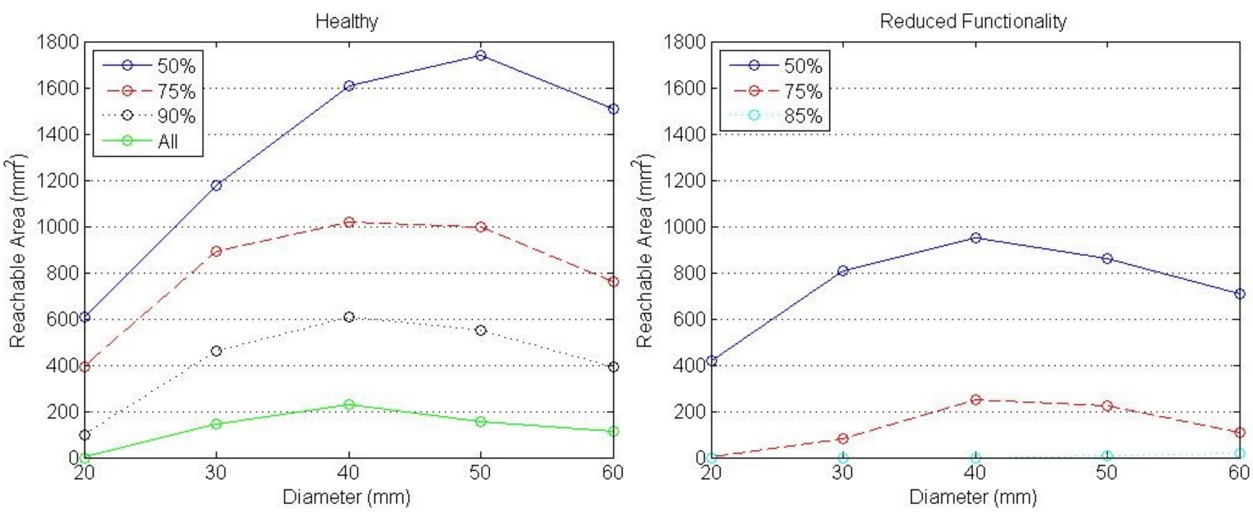

Figure 37. Summary values of the total amount of reachable area on each half cylinder as plotted by the percentage of each group that could reach the points

4.4 Discussion

4.4.1 Mapping the WFS to Object

A unique aspect of the WFS model was that it presented information about the functional ability of the hand in a 3D frame of reference. This allowed the WFS model to be mapped to the same space as any 3D-modeled handheld object. The mapping of functional abilities to the 3D space of the object showed that each of the functional weighting parameters had a distinct pattern of highest values on the surface of the cylinder.

The mappings represented the entire range of possible fingertip placements on the surface of the object, but in practice of grasping the object, only one fingertip placement will be used by each finger. Thus, the purpose of interpreting the different patterns of weighting was to identify the surface areas of highest functionality within a single finger. For example, while the *range of orientation angles* weighting in Figure 32 showed the highest overall values for the middle finger, only one of those surface points would be the fingertip placement of the middle finger for given grasp. Therefore, in using the WFS for making design decisions, the areas of highest functional values were identified. In the cylinder example for the representative healthy individual, the weightings of highest value were on the top for the *number of ways to reach* and the *range of orientation angles* weightings, and on the side for the *FAD range* angles weighting. Because a cylinder is axially symmetric, the axial location of areas of highest functionality were irrelevant, but the longitudinal location of highest functionality could be important for design features such as the device length, or the location of pertinent visual cues such as labeling. Further, the pattern of weightings would play a larger role in asymmetric objects, because the positioning of the object in the hand would be more stringently defined.

There are a few constraints to this mapping process that were identified during interpretation of the resulting data, and should be considered for future use for both healthy and RF model mapping. First, the fingers were mapped to the cylinder surface independently which resulted in overlapping regions mapped on the surface of the object. While it is possible for two different fingers to touch the same point at different times, no two fingers could contact the same point at the same time. This was inconsequential for the surface of the cylinder where minimal overlap occurred and only in areas with low functional values, but should be considered for more complex surfaces. Second, there is no finger-object interference detection implemented in the current model. The result of this is that the mapping may be providing an overestimation of the hands abilities, particularly for large objects. Future work will address these limitations.

4.4.2 Design Variation with WFS Model

The mapping of WFS models to the varying diameters of cylinder showed that there were both qualitative and quantitative trends that could be used to design the object. Qualitatively, it was shown that as the diameter of the cylinder was changed, the location on the cylinder where the highest values of the functional weightings changed. While the area of highest functionality remained near the top of the cylinder for the *number of ways to reach* weighting and near the sides of the cylinder for the *range of FAD angles* weighting, it moved from the top of the cylinder to the sides of the cylinder as cylinder diameter was increased for the *range of orientation angles* weighting. In this case, because of the axial symmetry of the cylinder, the change had little effect on the choice of the diameter. However, it was important to note that the weighting patterns changed with varying dimensions because they will also change when mapped to other objects that may not be symmetric.

Quantitatively, the differences in mappings of the WFS on the cylinder models were used to identify the best diameter of the device to be gripped in a power grasp for both groups. The data showed that for maximum cumulative ability of all four fingers of the healthy group, the 40 mm diameter cylinder was best for a grasp that required either a large redundancy in the number of ways to reach the surface or a range of possible fingertip orientations on the surface, and the 30 mm diameter was best for a grasp that required a range of FADs on the surface. However, in comparison to the healthy group, the optimal diameters shifted for the functional abilities of the RF group. For the RF group, the diameter best for a power grasp using the highest levels of redundancy in placing the fingertip was 20 mm, the best for utilizing a range of fingertip positions was 50 mm, and the best for applying a range of forces was 40 mm. While this could be interpreted to mean that no single diameter was best, the results should be framed in the context of the needs of the device in order to choose the diameter that best fits the needs of the user/device interaction. The user of an auto-injector needs to be able to effectively grab the device, hold it firmly with fingertips flush to the surface, and oppose a variety of forces, so the functional weightings should bear a balanced weighting in the analysis. Based on this interpretation of the grasp context, it would be recommended for both the healthy and RF groups to have an auto-injector with a diameter of 40 mm. For the healthy group, this diameter would allow the average healthy user the highest number of ways to position the fingertip on the device, the highest range of angles in applying the fingertips to the surface, and the second highest range of angles with which to apply forces of the diameters presented. For the RF group, this diameter would allow the average RF user the second highest number of ways to position the fingertip on the device, the second highest range of angles in applying the fingertips to the surface, and the highest range of angles with which to apply forces of the diameters presented.

In this way, objective data from real humans can be used to support design decisions for handheld objects. This method can be applied to any individual or group of individuals that can be measured for hand dimensions and finger joint ROMs and to any object that can be modeled as a set of surface points. The computational nature of the process means that many design iterations can be tested without the need to physically prototype each design and test it with an individual or group of individuals. Further, it shows not only what the best objective options are, but what tradeoffs are being made for other design alternatives. For example, for the healthy group, a 30mm diameter could be chosen, such that it maximized the hand's ability to apply forces in a variety of directions, but that would come at the cost of having decreases in the number ways for the fingers to reach the device and the range of possible fingertip orientation angles on the surface with respect to the 40 mm diameter.

The total reachable areas showed that as the diameter of the cylinder increased, so did the average reachable area for both groups. This was credited primarily to the increase in overall surface area of the cylinder. However, while the surface area of the side of any cylinder increases proportional to the radius, the total amount of reachable surface did not follow a linear trend. This was attributed to the fact that the cylinders were becoming too large for the fingertips to reach all the way around the surface of the object. Spatially, the larger reachable areas corresponded to the surface of the object interacting with the wider "splay" section of each finger's reachable space that occurred due to abduction and adduction of the fingers. This splay was limited at larger MCP flexion values due to the physical constraints of the hand modeled in the WFS model, resulting in a more planar reachable space when the MCP joint was more flexed. While the total average reachable area values could be used to explain what objects can and cannot be reached by the average person, the averaging process simplifies the spatial complexities of the reachable space, and may over-represent larger diameters that are only reachable by larger hands. For this reason, the group model mappings provided a more accurate representation of the groups' abilities to reach the surfaces of the cylinders.

While the results of this research have been shown for an auto-injector, the mapping of WFS models to handheld objects has potential for any handheld device. The ability to map the abilities of the hands to objects and influence the design can be used to optimize design of objects ranging from videogame controllers to robotic assisted surgery controls and drone aircraft controls. Putting the controls of such devices in the reachable motion and force space allows for the insurance of complete control. In addition, with the availability of 3D printing, this mapping process has the potential to be used to design objects to accommodate specific individuals with customized casings for handheld objects such as the auto-injector or videogame controls.

In addition, this mapping process could also be used for design of other aspects of the auto-injector, such as the button placement. This work was not specifically performed with that analysis in mind, as the thumb motion patterns were not included, but insights could still be garnered from this approach. Specifically, if a squeeze button were to be used instead of a button on the end of the cylinder, it would be advised to have the button actuated by the index or middle finger. This is based on the fact that the mapping values for the index and middle fingers were the most consistent to reach around the device and produced the highest weighting values.

4.4.3 Universal Design using the Group Models

The mappings of the group models on the cylinders were presented to demonstrate the potential of the group models for universal design of handheld objects for a given population. The similarities and differences that the two groups produced were interpreted for design of a handheld object.

The primary qualitative difference between the two groups was the disparity in the ability of the little finger to reach the larger diameter cylinders. The inability of the little finger to reach the top of the 60 mm cylinder was attributed to the combination of lower ROMs in the RF group, and the little finger being the shortest finger. In practice, this meant that the fingertip of the little finger was theoretically less capable of contributing to grasping large diameter cylinders for the RF group. It should also be noted that the reachable volume of the little finger may also be underestimated for both groups due to the modeling assumption that the palm acted as a single rigid body. It has been shown in the past that this is not strictly the case [32], but the assumption of the palm as a rigid body was necessary given the data collection procedures.

The quantitative data showed that for the RF group, as the percentage of the population able to reach the cylinder surface increased, the most reachable diameters shifted to the higher diameter values. While the most reachable diameter for the >75% RF group was 40 mm, the second most reachable diameter was 50 mm, and the 30 mm diameter showed a reachable area of less than half of the 50 mm area. The only two diameters that showed any reachable area for the >85% group were the 50 mm and 60 mm diameters. This indicated that while the 40 mm diameter cylinder was the most reachable for >75% of the group, it is recommended that cylinders designed to be grasped in a power grasp by RF individuals be *at least* 40 mm in diameter.

While developed in different ways, and measuring different outcomes, the trends from these data bear a resemblance to the maximum grip strength data for a power grasp. Research has shown that for a power grasp, the maximum grip strength is achieved at a diameter between 30-40 mm [46,47]. Those grip force measurements were developed from a completely different set of experimental subjects and measurements, but the outcomes were similar because of the same underlying structure of the hand. However, while reproduction of the force magnitude results for different shapes of devices or grasps would require building customized measurement devices for each shape and experimental participants, all that would be required reproduction of the results for the WFS mapping would be digital 3D-models of the devices.

The influence of hand size on the group WFS model should also be considered when interpreting the mapping of the group models to the object surface. In general, larger hands were able to reach larger regions of space and consequently represent the largest areas of the group models, particularly for the larger diameter cylinders. The effect of this was that the reachable areas on larger diameter cylinders were primarily from the participants with larger hands in the group. The best example of this was in the healthy group model mappings where the >50% group data showed higher values for reachable area at the 50mm diameter when all other more restrictive subsections of the data (>75%, >90%, 100%) showed the highest values at 40mm diameter. Effectively, difference in the data from the >50% in comparison to the other groups was the removal of the data from the smaller hands that could not reach as much area on the larger cylinders. Therefore, it is recommended that the highest levels of inclusion (>75% or greater) be used for evaluation of the design using the group models. If a smaller subsection is required based on the mappings from a given group (>50% or less), it should be acknowledged that larger hands may be over-represented in the group model.

4.5 Conclusions

This research showed that the data contained in the WFS model can be applied to the surface of a 3D-modeled object, and that mapping can indicate the different ways that a fingertip can interact with an object in the hand. This means that the abilities of the hand can be mapped to the 3D model of any handheld object for evaluation during the design of the object without the need to prototype a physical model.

The results further showed that variations of a single design can be evaluated to objectively determine which variation best fits the abilities of an individual's hand or a group of individuals' hands. The WFS model has the potential to be used to computationally test object designs for a variety of different hand sizes and abilities before making physical prototypes. In doing so, the tradeoffs of the different functional weighting parameters can be balanced to best fit the desired task and grasp of the object.

The research also showed that the group models developed from the combination WFS models of individuals can be used to determine what percentage of the group will be able to grasp and touch an object at specific points on the surface. For the example case of the auto-injector these group models showed that 40 mm was the most universally reachable diameter of cylinder for a power grasp for both the healthy and RF groups. This type of information can be implemented to develop handheld objects that can be manipulated by the largest range of individuals possible. Specifically for the RF population, this can be used to design handheld objects so that people with a reduction in functionality can grasp and manipulate handheld objects needed for extending independence.

5. CONCLUSIONS

This research sought to develop a better understanding of hand function through the development and application of a novel kinematics-based model of the spaces reachable by the fingers on the hand. The WFS model development, the application of the model to healthy and RF groups, and the mapping of the experimental models to the surface of a 3D-modeled object each provided a unique perspective to the understanding of hand function.

The results of the model development showed that the WFS modeling process was capable of calculating novel measures of functionality representative of hand capabilities in 3D space. The experimental models showed similarity in weighting spaces and patterns with the 50^{th} percentile male theoretical model. Each of the three weighting parameters displayed unique patterns that were similar across all of the models which indicated that different reachable spaces may be used based on the requirements of the grasping task. In addition, the models showed individual variation in sizes, shapes, and weighting values that indicated potential for the models to be applied in evaluation of hand function.

The data comparison from the healthy and RF groups showed both similarities and significant differences between the groups that could be applied to improving clinical evaluation and use of the RF hand. The ROM data showed that the main differences between the healthy and RF groups were in the flexion and extension ranges of the finger joints and not the abduction and adduction ranges, indicating that 2D plots may be sufficient for evaluation of the changes in function. The WFS model data showed qualitative differences in size and shape of the reachable areas between the two groups and quantitative differences between the maximum values of the weighting parameters and total reachable volume of the two groups. These differences indicated that the WFS model was capable of detecting changes in hand function between individuals with varying levels of functionality. In addition, it was also noted that size of the hand had influences on the total reachable area and *number of ways to reach* weighting that should be noted when making comparisons between individuals. The two group models showed that universally reachable spaces existed for the healthy group, but no regions in space were universally reachable by all of the individuals in the RF group. However, the areas that were most reachable for the RF group overlapped with the healthy group's universally reachable regions indicating that those areas are the most universally reachable for both groups.

Mapping the WFS model to the surface of the cylinder showed the potential of the model to be used for design of handheld objects. The data showed that the WFS model could be mapped to a series of points representing the surface of a handheld object to display the potential interactions of the fingertips with the object. By varying the diameter of the cylindrically shaped auto-injector it was possible to objectively evaluate the best diameter based on the hand's ability to interact with the surface for a given task. This evaluation was shown to be possible for specific individuals as well as both healthy and RF groups of individuals. In addition, when mapped to the cylinder surface, the group models were shown to be able to determine the most universally reachable designs for the auto-injector for both the healthy and RF groups.

Future work will focus on expanding the accessibility of the WFS model, implementing force magnitude measurements, examining the underlying limitations in the modeling process, and implementing the mapping process to better understand human motor control. Currently, the ROM measurements are made through motion capture technology that is not widely available for many clinicians. Therefore, the model will be tested with ROM measurements made from goniometers commonly available to clinicians to determine if the goniometers provide the accuracy needed for the WFS model to detect and present significant changes in a clinical environment. Next, the current iteration of the WFS model addresses the directionality of force generation but not the magnitude, so the addition of force magnitude data will be implemented in future iterations of this work. In addition, further research will examine any potential gains from addressing limitations of the model, namely the assumption that the palm acts as a rigid body. Finally, the process of mapping the WFS model to objects has the potential to be used as a framework to understand how and why people grasp objects the ways that they do. Experimentally measured grasps will be evaluated with respect to the WFS model mappings to investigate the potential influence the functional weightings have on the optimization processes that the body uses to choose grasping strategies and finger placements.

In conclusion, this research presents the development, analysis, and potential applications of a new model of hand function in 3D space. The WFS model can provide the foundation for evaluation of hand function and aid in design of handheld objects. Finally, through the combination of evaluation and design, the WFS model has the potential improve lives and extend independence for RF individuals by designing handheld objects specifically to match the abilities of the RF hand.

REFERENCES

REFERENCES

[1] Verbrugge, L. M., and Patrick, D. L., 1995, "Seven chronic conditions: their impact on US adults' activity levels and use of medical services.," Am. J. Public Health, **85**(2), pp. 173–82.

[2] Covinsky, K. E., Lindquist, K., Dunlop, D. D., Gill, T. M., and Yelin, E., 2008, "Effect of arthritis in middle age on older-age functioning.," J. Am. Geriatr. Soc., **56**(1), pp. 23–8.

[3] Verbrugge, L. M., Lepkowski, J. M., and Konkol, L. L., 1991, "Levels of disability among U.S. adults with arthritis.," J. Gerontol., **46**(2), pp. S71–83.

[4] Dellhag, B., and Bjelle, a, 1999, "A five-year followup of hand function and activities of daily living in rheumatoid arthritis patients.," Arthritis Care Res., **12**(1), pp. 33–41.

[5] Chung, K. C., Pillsbury, M. S., Walters, M. R., and Hayward, R. a, 1998, "Reliability and validity testing of the Michigan Hand Outcomes Questionnaire.," J. Hand Surg. Am., **23**(4), pp. 575–87.

[6] Beaton, D. E., Katz, J. N., Fossel, a H., Wright, J. G., Tarasuk, V., and Bombardier, C., 2001, "Measuring the whole or the parts? Validity, reliability, and responsiveness of the Disabilities of the Arm, Shoulder and Hand outcome measure in different regions of the upper extremity.," J. Hand Ther., **14**(2), pp. 128–46.

[7] Demirbilek, O., and Demirkan, H., 2004, "Universal product design involving elderly users: a participatory design model.," Appl. Ergon., **35**(4), pp. 361–70.

[8] Clarkson, P. L. P. J., and Robinson, P., 2010, Designing Inclusive Interactions, Springer London, London.

[9] Bix, L., de la Fuente, J., Pimple, K. D., and Kou, E., 2009, "Is the test of senior friendly/child resistant packaging ethical?," Health Expect., **12**(4), pp. 430–7.

[10] Carmeli, E., Patish, H., and Coleman, R., 2003, "The aging hand," Journals Gerontol. Ser. a-Biological Sci. Med. Sci., **58**(2), pp. 146–152.

[11] Rønningen, A., and Kjeken, I., 2008, "Effect of an intensive hand exercise programme in patients with rheumatoid arthritis.," Scand. J. Occup. Ther., **15**(3), pp. 173–83.

[12] Ranganathan, V. K., Siemionow, V., Sahgal, V., and Yue, G. H., 2001, "Effects of aging on hand function.," J. Am. Geriatr. Soc., **49**(11), pp. 1478–84.

[13] Carpinella, I., Jonsdottir, J., and Ferrarin, M., 2011, "Multi-finger coordination in healthy subjects and stroke patients: a mathematical modelling approach," J. Neuroeng. Rehabil., **8**.

[14] Carpinella, I., Mazzoleni, P., Rabuffetti, A., Thorsen, R., and Ferrarin, M., 2006, "Experimental protocol for the kinematic analysis of the hand: Definition and repeatability," Gait Posture, **23**(4), pp. 445–454.

[15] Zhou, H. Y., and Hu, H. S., 2008, "Human motion tracking for rehabilitation-A survey," Biomed. Signal Process. Control, **3**(1), pp. 1–18.

[16] Su, F. C., Kuo, L. C., Chiu, H. Y., and Chen-Sea, M. J., 2003, "Video-computer quantitative evaluation of thumb function using workspace of the thumb," J. Biomech., **36**(7), pp. 937–942.

[17] Cruz, E. G., Waldinger, H. C., and Kamper, D. G., 2005, "Kinetic and kinematic workspaces of the index finger following stroke.," Brain A J. Neurol., **128**(Pt 5), pp. 1112–21.

[18] Kuo, L. C., Chiu, H. Y., Chang, C. W., Hsu, H. Y., and Sun, Y. N., 2009, "Functional workspace for precision manipulation between thumb and fingers in normal hands," J. Electromyogr. Kinesiol., **19**(5), pp. 829–839.

[19] Dragulescu, D., Perdereau, V., Drouin, M., Ungureanu, L., and Menyhardt, K., 2007, "3D active workspace of human hand anatomical model," Biomed. Eng. Online, **6**.

[20] Zheng, R., and Li, J., 2010, "Kinematics and workspace analysis of an exoskeleton for thumb and index finger rehabilitation," 2010 IEEE International Conference on Robotics and Biomimetics, pp. 80–84.

[21] Greiner, T., 1991, "Hand anthropometry of US army personnel," Security, **TR-92/011**, p. 434.

[22] Porter, R. S., and Kaplan, J. L., 2011, The Merck Manual for Health Care Professionals.

[23] Lin, J., Wu, Y., and Huang, T. S., 2000, "Modeling the constraints of human hand motion," IEEE Proc. from Work. Hum. Motion, pp. 121–126.

[24] Lee, J. T., and Kunii, T. L., 1995, "Model-based analysis of hand posture," IEEE Comput. Graph. Appl., **15**(5), pp. 77–86.

[25] Brand, P. W., and Hollister, A. M., 1999, Clinical Mechanics of the Hand, Mosby, Inc.

[26] Denavit, J., and Hartenberg, R. S., 1955, "A kinematic notation for lower pair mechanisms," Appl. Mech., **22**, pp. 215–221.

[27] Spong, M. W., Hutchinson, S., and Vidyagasar, M., 2006, Robot Modeling and Control, John Wiley & Sons, Inc.

[28] Santos, V. J., and Valero-Cuevas, F. J., 2006, “Reported anatomical variability naturally leads to multimodal distributions of Denavit-Hartenberg parameters for the human thumb,” IEEE Trans. Biomed. Eng., **53**(2), pp. 155–163.

[29] Johnson, R., Yang, J., and Long, J., 2010, “Finger reach envelope using the marching cubes method,” J. Hum. Factors Model. Simul., **1**(3), pp. 321–338.

[30] Tang, J., Zhang, X. D., and Li, Z. M., 2008, “Operational and maximal workspace of the thumb,” Ergonomics, **51**(7), pp. 1109–1118.

[31] Wu, G., van der Helm, F. C. T., Veeger, H. E. J., Makhsous, M., Van Roy, P., Anglin, C., Nagels, J., Karduna, A. R., McQuade, K., Wang, X. G., Werner, F. W., and Buchholz, B., 2005, “ISB recommendation on definitions of joint coordinate systems of various joints for the reporting of human joint motion - Part II: shoulder, elbow, wrist and hand,” J. Biomech., **38**(5), pp. 981–992.

[32] El-shennawy, M., Nakamura, K., Patterson, R. M., and Viegas, S. F., 2001, “Three-dimensional kinematic analysis of the second through fifth carpometacarpal joints,” J. Hand Surg. Am., **26**(6), pp. 1030–1035.

[33] Li, Z. M., Kuxhaus, L., Fisk, J. A., and Christophel, T. H., 2005, “Coupling between wrist flexion-extension and radial-ulnar deviation,” Clin. Biomech., **20**(2), pp. 177–183.

[34] Helmick, C. G., Felson, D. T., Lawrence, R. C., Gabriel, S., Hirsch, R., Kwoh, C. K., Liang, M. H., Kremers, H. M., Mayes, M. D., Merkel, P. a, Pillemer, S. R., Reveille, J. D., and Stone, J. H., 2008, “Estimates of the prevalence of arthritis and other rheumatic conditions in the United States. Part I.,” Arthritis Rheum., **58**(1), pp. 15–25.

[35] Roger, V. L., Go, A. S., Lloyd-Jones, D. M., Benjamin, E. J., Berry, J. D., Borden, W. B., Bravata, D. M., Dai, S., Ford, E. S., Fox, C. S., Fullerton, H. J., Gillespie, C., Hailpern, S. M., Heit, J. a, Howard, V. J., Kissela, B. M., Kittner, S. J., Lackland, D. T., Lichtman, J. H., Lisabeth, L. D., Makuc, D. M., Marcus, G. M., Marelli, A., Matchar, D. B., Moy, C. S., Mozaffarian, D., Mussolino, M. E., Nichol, G., Paynter, N. P., Soliman, E. Z., Sorlie, P. D., Sotoodehnia, N., Turan, T. N., Virani, S. S., Wong, N. D., Woo, D., and Turner, M. B., 2012, “Heart disease and stroke statistics--2012 update: a report from the American Heart Association.,” Circulation, **125**(1), pp. e2–e220.

[36] Luckhaupt, S., and Dahlhamer, J., 2012, “Prevalence and work-□relatedness of carpal tunnel syndrome in the working population, United States, 2010 national health interview survey,” Am. J. Ind. Med., (March), pp. 1–10.

[37] Jackson, L., 2001, “Non-fatal occupational injuries and illnesses treated in hospital emergency departments in the United States,” Inj. Prev., **7**(Suppl I), pp. i21–26.

[38] Vermeulen, G. M., Slijper, H., Feitz, R., Hovius, S. E. R., Moojen, T. M., and Selles, R. W., 2011, “Surgical management of primary thumb carpometacarpal osteoarthritis: a systematic review.,” J. Hand Surg. Am., **36**(1), pp. 157–69.

[39] Theilig, S., Podubecka, J., Bösl, K., Wiederer, R., and Nowak, D. a, 2011, “Functional neuromuscular stimulation to improve severe hand dysfunction after stroke: does inhibitory rTMS enhance therapeutic efficiency?,” Exp. Neurol., **230**(1), pp. 149–55.

[40] Kurillo, G., Gregoric, M., Goljar, N., and Bajd, T., 2005, “Grip force tracking system for assessment and rehabilitation of hand function.,” Technol. Health Care, **13**(3), pp. 137–49.

[41] Leitkam, S. T., Bush, T., and Bix, L., 2013, “Determining Functional Finger Capabilities of Healthy Adults: Comparing Experimental Data to a Biomechanical Model.,” J. Biomech. Eng., **136**(February), pp. 1–11.

[42] Eberhardt, K., Johnson, P. M., and Rydgren, L., 1991, “The occurrence and significance of hand deformities in early rheumatoid arthritis.,” Br. J. Rheumatol., **30**(3), pp. 211–3.

[43] Youm, Y., Gillespie, T. E., Flatt, a E., and Sprague, B. L., 1978, “Kinematic investigation of normal MCP joint.,” J. Biomech., **11**(3), pp. 109–18.

[44] Li, Z. M., Kuxhaus, L., Fisk, J. A., and Christophel, T. H., 2005, “Coupling between wrist flexion-extension and radial-ulnar deviation,” Clin. Biomech., **20**(2), pp. 177–183.

[45] Dias, J. J., Smith, M., Singh, H. P., and Ullah, A. S., 2009, “The Working Space of the Hand in Rheumatoid Arthritis: Its Impact on Disability,” J. Hand Surgery-European Vol., **34E**(4), pp. 465–470.

[46] Kong, Y.-K. K., and Lowe, B. D., 2005, “Optimal cylindrical handle diameter for grip force tasks,” Int. J. Ind. Ergon., **35**(6), pp. 495–507.

[47] Edgren, C. S., Radwin, R. G., and Irwin, C. B., 2004, “Grip Force Vectors for Varying Handle Diameters and Hand Sizes,” Hum. Factors J. Hum. Factors Ergon. Soc., **46**(2), pp. 244–251.